AD-A173 736 STUDY OF GROWN-IN DEFECTS VERSES GROWTH PARAMETERS IN GAAS AND AL(X)GA(1-.. (U) FLORIDA UNIV GAINESVILLE DEPT OF ELECTRICAL ENGINEERING S S LI 15 JUN 85 1/1

UNCLASSIFIED AFOSR-TR-86-0676 AFOSR-81-0187 F/G 20/2 NL

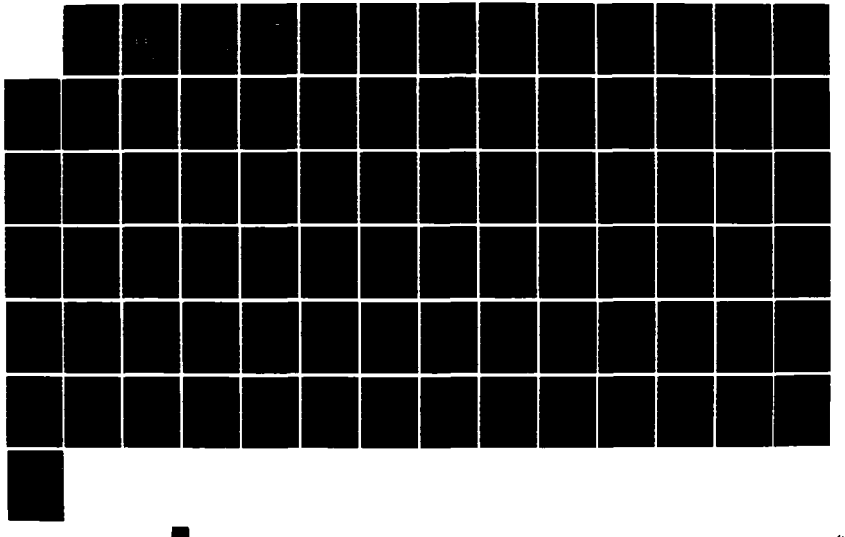

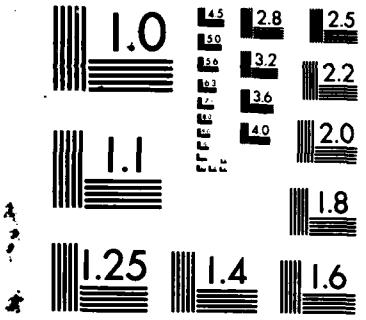

(2)

Annual Technical Report
(covered period from June 11, 1984 to June 10, 1985)

Study of Grown-in Defects vs. Growth Parameters in GaAs and $Al_xGa_{1-x}As$ Epitaxial Films Grown by LPE and MOCVD Techniques

Submitted to

Air Force Office of Scientific Research
Bolling AFB, D.C.20234

Approved for public release;
distribution unlimited.

College of Engineering

UNIVERSITY OF FLORIDA

Gainesville, Florida

(2)

AFOSR Grant No. AFOSR-81-0187

Annual Technical Report
(covered period from June 11, 1984 to June 10, 1985)

Study of Grown-in Defects vs. Growth Parameters in GaAs and $Al_xGa_{1-x}As$ Epitaxial Films Grown by LPE and MOCVD Techniques

Submitted to

Air Force Office of Scientific Research
Bolling AFB, D.C.20234

Prepared by

Sheng S. Li
Professor

Department of Electrical Engineering
University of Florida

Gainesville, FL. 32611

June 15, 1985

SECURITY CLASSIFICATION OF THIS PAGE (When Data Entered)

REPORT DOCUMENTATION PAGE		READ INSTRUCTIONS BEFORE COMPLETING FORM
1. REPORT NUMBER AFOSR-TR- 86-0676	2. GOVT ACCESSION NO.	3. RECIPIENT'S CATALOG NUMBER
4. TITLE (and Subtitle) "STUDY OF GROWN-IN DEFECTS VS. GROWTH PARAMETERS IN GaAs AND AlxGa1-xAs EPITAXIAL FILMS GROWN BY LPE AND MOCVD TECHNIQUES"		5. TYPE OF REPORT & PERIOD COVERED ANNUAL, 11JUN84 - 10JUN85 6. PERFORMING ORG. REPORT NUMBER
7. AUTHOR(s) LI, SHENG S.		8. CONTRACT OR GRANT NUMBER(s) AFOSR-81-0187
9. PERFORMING ORGANIZATION NAME AND ADDRESS UNIV OF FLORIDA Electrical Engineering Dept Gainesville FL 32611		10. PROGRAM ELEMENT, PROJECT, TASK AREA & WORK UNIT NUMBERS 61102F 2306/B1
11. CONTROLLING OFFICE NAME AND ADDRESS AFOSR/NE Bolling AFB DC 20332-6448		12. REPORT DATE June 15 85 13. NUMBER OF PAGES 75
14. MONITORING AGENCY NAME & ADDRESS(if different from Controlling Office) AFOSR/NE		15. SECURITY CLASS. (of this report) Unclassified 15a. DECLASSIFICATION/DOWNGRADING SCHEDULE

16. DISTRIBUTION STATEMENT (of this Report)

Approved for public release;
distribution unlimited.

17. DISTRIBUTION STATEMENT (of the abstract entered in Block 20, if different from Report)

18. SUPPLEMENTARY NOTES

19. KEY WORDS (Continue on reverse side if necessary and identify by block number)

20. ABSTRACT (Continue on reverse side if necessary)

Study on the native defects in GaAs and $Al_xGa_{1-x}As$ grown under the various conditions have been made. Fires, a model for describing the physical origins of the EL2 center in GaAs is presented based on the kinetic reaction equations and the analysis of electric-field enhanced emission rates for the four different types of potential well. It has been shown that the EL2 center may be ascribed to two different types of native defect: One level (E_c-0.83 eV) attributing to the antisite defect, As_{Ga} or the antisite cluster, As_{Ga}-As_4 is designated as the EL2a electron trap, and the other level

DD FORM 1 JAN 73 1473 EDITION OF 1 NOV 65 IS OBSOLETE

U/C

SECURITY CLASSIFICATION OF THIS PAGE (When Data Entered)

(E_c-0.76 eV) attributing to the antisite-vacancy complex, As_{Ga}-V_{As} is designated as the EL2b electron trap.. The EL2a electron trap was found to be strongly dependent on the growth condition, e.g., (AsH_3)/(TMGa) ratio growth temperature growth rate (mainly at lower growth rate) and buffer layer. Second, the final transition state of electron emission from the DX center to the nonspherical conduction band minima in $Al_xGa_{1-x}As$ has been studied by capacitance-voltage measurement and Deep level Transient Spectroscopy experiment. The results indicate that the conduction band minimum associated with the electron emission is the L band instead of the band which is lowest conduction band. Analysis of the electric-field enhanced emission rate applied to the Coulombic and Yukawa potential well has further supported the fact that emission and capture of electron from the DX center is related to the L minimum in the conduction band.

Abstract

Study on the native defects in GaAs and $Al_xGa_{1-x}As$ grown under the various conditions has been made. First, a model for describing the physical origins of the EL2 center in GaAs is presented based on the kinetic reaction equations and the analysis of electric-field enhanced emission rates for the four different types of potential well. It has been shown that the EL2 center may be ascribed to two different types of native defect: One level (E_c-0.83 eV) attributing to the antisite defect, As_{Ga} or the antisite cluster, As_{Ga}-As_4 is designated as the EL2a electron trap, and the other level (E_c-0.76 eV) attributing to the antisite-vacancy complex, As_{Ga}-V_{As} is designated as the EL2b electron trap. The EL2a electron trap was found to be strongly dependent on the growth condition, e.g., [AsH_3]/[TMGa] ratio, growth temperature growth rate (mainly at lower growth rate) and buffer layer. Second, the final transition state of electron emission from the DX center to the nonspherical conduction band minima in $Al_xGa_{1-x}As$ has been studied by capacitance-voltage measurement and Deep level Transient Spectroscopy experiment. The results indicate that the conduction band minimum associated with the electron emission is the L band instead of the band which is the lowest conduction band. Analysis of the electric-field enhanced emission rate applied to the Coulombic and Yukawa potential well has further supported the fact that emission and capture of electron from the DX center is related to the L minimum in the conduction band.

TABLE OF CONTENTS

CHAPTER I
INTRODUCTION

A study of deep level defects in semiconductors is extremely important, since the presence of defects significantly affects the device performance. For electronic devices, the deep level defects could increase the leakage current and reduce the gain of transistors. For photonic devices, nonradiative deep centers act as a lifetime killer and reduce the sensitivity and the luminescence efficiency. Thus, the origins of defects must be investigated in order to control the defects and improve the device performance.

The native point defects and grown-in defects are frequently present in III-V compounds in the 10^{15}- 10^{16} cm^{-3} concentration range. Up to now, however, no clear identification has been made. This might be partly due to the fact that, besides simple point defects like vacancies and interstitials, certain kinds of defect complexes also exist especially in binary and ternary compound materials. Furthermore, it has been shown that these kinds of defects are strongly dependent on the growth techniques and growth conditions.

The purpose of this report is to perform a detailed analysis of the grown-in defects in GaAs and $Al_xGa_{1-x}As$ which is essential for optimization of material growth by various techniques under different growth condition. The main objectives of this study are

(1) To derive a theoretical model of the EL2 center in GaAs

grown by MOCVD and VPE, based on the analysis of kinetic reaction equations and electric field enhanced emission rates, in order to identify the physical origins, the type of potential well and the charge state;

(2) to make a correlation of depth profile for the dominant deep-level defects to various growth parameters (mole fraction of trimethylgallium to arsine, growth temperature, growth rate) in MOCVD grown multiepilayer GaAs;

(3) to identify the final transition state of electron emission (capture) associated with nonspherical conduction band minima for the DX center in $Al_xGa_{1-x}As$, and to predict its potential well and charge state.

Chapter II reviews the native defects and complexes in GaAs and $Al_xGa_{1-x}As$, emphasizing the EL2 center and the DX center. In Chapter III, the preparation of GaAs and $Al_xGa_{1-x}As$ specimens grown by various techniques under different growth condition, and the experimental details are described. Experimental tools used in this study include the current-voltage, capacitance-voltage, a. c. admittance, thermally stimulated capacitance and deep level transient spectroscopy measurements. Chapter IV develops a theoretical model for the physical origins of the EL2 center in GaAs and a prediction of the final transition state of electron emission and capture from the DX center in $Al_xGa_{1-x}As$. In addition, an analysis of the electric field enhanced emission rates for the both kinds of defect center is made to determine the type of potential well and charge state. In Chapter V, the physical origins of the EL2 center and the nature of electron

transition associated with the DX center are depicted, based on the theoretical and experimental results. Study of the grown-in defects in multi-epilayer GaAs (with/without a buffer layer) grown by MOCVD under different [AsH_3]/[TMGa] ratios, growth temperatures and growth rates is depicted in Chapter VI. Summary and conclusions are given in Chapter VII.

CHAPTER II
REVIEW OF NATIVE DEFECTS AND COMPLEXES IN GALLIUM ARSENIDE AND ALUMINUM GALLIUM ARSENIDE

There are a number of possible native defects and complexes in binary and ternary compound semiconductors such as GaAs and $Al_xGa_{1-x}As$. In addition to these native defects, impurity atoms and the complexes of native defects may also be expected when impurity atoms are incorporated, as is shown in table 2.1. In this study, attention will be focused on the key point defects such as the EL2 center in GaAs and the DX center in $Al_xGa_{1-x}As$ which play an important role in determining the electrical properties of these materials. Unfortunately, these defects are somewhat uncontrollable, and have not been identified with any confidence.

2.1. Gallium Arsenide

A survey of the literature [1-15] on the subject of defects in GaAs grown by various techniques has shown that only a few electron and hole traps are common point defects observed in both the bulk and epitaxial layer. Among them, the EL2 level with activation energy ranging from E_c-0.75 eV to E_c-0.83 eV is the dominant midgap electron trap in GaAs. This trap has been observed in GaAs grown by Bridgmann, liquid phase encapsulation (LEC), vapor phase epitaxy (VPE), and metalorganic chemical vapor deposition (MOCVD) techniques as well as in high temperature heat-treated GaAs specimen. In earlier study,

Table.2.1. Parametric identification of defects in the GaAs and AlGaAs.

Type of Experiment	Defect	Reference
Variation of Growth Condition	Electron Trap in VPE GaAs	[1] [2]
	Electron Trap in LPE GaAs	[3]
	Electron Trap in MOCVD GaAs	[4] [5]
Change of Dopant	DX Center in AlGaAs	[16] [17]
Compositional Variation in Ternary Compounds	Electron Irrad. and Native Defect in LPE AlGaAs	[18]
	Luminescent center in AlGaAs	[19]
Hydrostatic Pressure	Electron Trap in GaAs	[6]
	DX Center in AlGaAs	[18]
Orientation-dependent Defect Production	Electron Irrad. Defect in GaAs	[8]
Energy of Incidental Electron	Electron Irrad. Defect in GaAs	[7]
Anisotrpic Cold Ionization	Electron Trap in GaAs	[20]

Lagowski et al.[9] proposed that the EL2 level was due to an arsenic antisite (As_{Ga}^{++}) defect on the basis of the effect of melt stoichiometry and the shallow donor impurities on the EL2 level concentration. This was further supported by the EPR and IR optical absorption measurements [10]. Watanabe et al.[11] suggested that there were two kinds of EL2 center in MOCVD grown GaAs epilayers. One is the E_c-0.83 eV (EL2a) level consisting of a Ga vacancy, an As antisite defect or its complex for the specimen grown at 720 to 740 ^{o}C. The other is the E_c-0.76 eV (EL2b) level consisting of a Ga vacancy, an interstitial As or its complex for GaAs grown at 630 to 660^{o}C.

Recently, by the optically detected electron nuclear double resonance (ODENDOR) measurements, Meyer et al.[12] reported that the EL2 defects were complexes of nearby As antisite defects, possibly involving other impurities. Furthermore, it has been shown that, in oxygen-doped or -implanted GaAs, there was another midgap electron trap (EL0 or EL20) having the same characteristics of emission rate versus temperature as that of the EL2 level, but having different value of electron capture cross section and optical properties. Lagowski et al.[13] found that the electron capture cross section of the EL0 level is about four times larger than that of the EL2 level by resolving the DLTS spectrum of oxygen-doped GaAs, and suggested that its origin could be an oxygen impurity atom in the arsenic site. In the optical transition from the stable state to the metastable state, Taniguchi et al.[14] also made a distinction between the EL20 level in oxygen-implanted LPE GaAs and the EL2 level in GaAs material grown by

various techniques. The above results strongly suggest that the EL2 center in GaAs may be attributed to more than two different types of native point defects with very close activation energies (so called, a EL2 family) [15]. Therefore, it is difficult to pin-point exactly what are the physical origins of the EL2 center.

2.2. Aluminum Gallium Arsenide

$Al_xGa_{1-x}As$, an important alloy system in the field of high-speed and opto-electronic devices is known to have a characteristic deep state, known as the DX center, in addition to other native defects, when the shallow donor impurities are incorporated with the native defect, as is shown in table 2.2. Among the unusual electrical and optical properties of the DX center, the most significant features are the large lattice relaxation conformed by observation of an abnormally large Stoke's shift resulting in persistent photoconductivity, the temperature dependent capture cross section for the electron, and the very high concentration comparable to that of incorporated dopant impurities.

To explain the extremely large lattice relaxation, Lang and Logan [16] have assumed that there is a defect state which is resonant with conduction band before the capture of an electron, but which relaxes to a point nearly 0.8 eV deep in the forbidden energy gap after the capture of an electron. In other word, the defect wave function has been treated as a sufficiently localized one, even when it is resonant in the continuum states of the band, to produce a very substantial lattice relaxation, i.e., non-effective-mass-like. Since any defect

Table 2.2. Electron traps in n-type AlGaAs.

Activation Energy(eV)	Growth Method	Remark	Reference
E_c-Ø.19	LPE	DX(Sn)	[16]
Ø.18	MBE		[21]
Ø.21	LPE	DX(Sn)	[17]
Ø.25	MOCVD		[22]
Ø.28	LPE,MOCVD	DX(S,Se,Te)	[16] [17]
Ø.31	MBE		[21]
Ø.32	MOCVD	DX(Te)	[23]
Ø.33	MOCVD	DX(Ge)	[17]
Ø.35	MOCVD		[22]
Ø.38	MOCVD		[24]
Ø.40	MBE	DX(Si)	[21] [25]
Ø.43	LPE,MOCVD	DX(Si,Te)	[16] [17]
Ø.45	MOCVD		[22]
Ø.47	MBE	DX(Si)	[29]
Ø.51	MBE		[21]
Ø.54	Be Implanted	DX(Be)	[26]
Ø.62	MOCVD		[24] [27]
Ø.63	MBE		[21]
Ø.66	MOCVD		[22]
Ø.71	MBE		[21]
Ø.77	MBE		[27]
Ø.82	MOCVD		[22] [24]
Ø.94	Neutron induced		[28]
1.22	MBE		[27]

resonance has a delocalized Bloch-wave component in its wave function in addition to a localized component, they have defined a localized resonant state to be one in which the corresponding electronic charge density is predominantly found in the immediate vicinity of the defect. In this view of deep levels, a strong lattice relaxation of the DX center has been explained as originated from a resonant state, such as the unoccupied DX center. On the basis of non-effective-mass theory, therefore, Lang and Logan have proposed a model in which the microstructure of DX-like center is a complex involving a donor impurity and an anion vacancy.

It is known that, under pressure, an energy band configuration of GaAs with respect to Γ, L and X minima becomes similar to that of AlGaAs alloy system, even without introducing any Al atom. For that reason, Mizuta et al. [18] have studied the DLTS spectra of GaAs under hydrostatic pressure and AlGaAs doped with Si, Se or Sn, in order to verify the interaction between the conduction band and the electronic state of the DX center. They observed that the features of the pressure-induced electron trap in GaAs, appeared at a critical pressure with a high concentration, are analogous to those of the DX center in AlGaAs (the appearance at a critical pressure and its high concentration). The change of thermal activation energy in Si-doped GaAs from 0.1 eV under normal condition to 0.3 eV under pressure has indicated that the observed trap has a characteristic of large lattice relaxation. Moreover, the fact that 100% of the incorporated Si in GaAs acts as shallow donors and that the free carriers are freezed out just below the temperature where the DLTS signal appears

are strongly suggestive that the trap itself is a source of free carriers. Therefore, Mizuta et al. have concluded that a shallow donor level due to a substitutional donor atom in GaAs becomes deep and behaves as the DX center when pressure higher than about 24 Khars is applied or when Al atoms fraction more than 24% are incorporated. As to the nature and origin of the DX center, even though a considerable effort has been devoted to identify the physical origin of this center, there still remains a serious discrepancy to be solved.

CHAPTER III
EXPERIMENTAL PROCEDURE

Samples of GaAs and $Al_xGa_{1-x}As$ grown by MOCVD technique under different growth conditions are studied by using current-voltage (I-V), capacitance-voltage (C-V), a.c. admittance, thermally stimulated capacitance (TSCAP), and deep level transient spectroscopy (DLTS) measurements. From these measurements, one can determine the electrical characteristics as well as the defect parameters such as energy levels, defect densities, temperature dependent capture cross sections, and nature of emission and capture of an electron from deep level traps associated with the conduction band minima in both materials.

3.1. Sample Preparation

GaAs specimens of multi-epilayer structures were grown by 1 atm. MOCVD under H_2 ambient. The crystal orientation was <100> tilted 2^o toward <110>. The epilayers were grown by altering the growth condition in a stepwise fashion. The $[AsH_3]/[TMGa]$ ratio was varied from 2.2 to 33; the growth temperature was varied between 580 to 675 ^oC, and the growth rate was fixed at 0.07 and 0.14 μm/min.. Samples OM-2-295, -296, and -309 were grown directly on the undoped semi-insulating (S.I.) GaAs substrate, whereas samples OM-2-310, -312, and -367B were grown with a 6 μm thick buffer layer on top of

the S.I. GaAs substrate. The epilayer in sample OM-2-367B was grown for shorter times, and consequently was thinner than the rest of the samples studied. Moreover, the buffer layer for this sample was not completely compensated as in the other samples. Table 3.1 summarizes the growth parameters for the six MOCVD grown samples used in this study. The unintentionally doped GaAs epilayers grown under As-rich condition were n-type with net doping densities ranging from $1x10^{14}$ to $6x10^{15}$ cm^{-3} depending on the growth conditions. The electrical properties and deep level defects are determined using Au-GaAs Schottky barrier structure.

$Al_xGa_{1-x}As$ specimens undoped or doped with Si, Sn, Be and Ge were grown by MOCVD and LPE technique under different growth condition, as is shown in table 3.2. The V/III ratio was around 20, while the Al composition ratios were varied from 30 to 41 %. The growth temperature was ranged from 650 to 800 ^{o}C for the purpose of analysizing the temperature dependent grown-in defects. Structures of p-n junction and Schottky barrier on the n-type GaAs substrate of <100> or <111> crystal orientation were used in this study. Whereas epilayers of Be- or Ge-doped AlGaAs were p-type, epilayers of undoped, Si- or Sn doped $Al_xGa_{1-x}As$ were n-type with net doping concentrations ranging from $3x10^{16}$ to $2x10^{18}$ cm^{-3}.

3.2. Current-Voltage Measurement

Measurements of the current-voltage (I-V) characteristics under forward bias condition yield useful information concerning the conduction mechanisms, recombination processes in the space charge

Table.3.1. Growth conditions for the six samples of unintentionally doped GaAs multi-epilayer structures grown by 1 atm MOCVD under H_2.

Samples (OM-2-)	Buffer Layer Thickness (μm)	Growth Conditions			Epilayer Thickness (μm)
		$[AsH_3]/[TMGa]$ Ratio	Growth Rate (μm/min.)	Growth Temp. (^oC)	
295	0	5.5-16.5	0.07-0.14	675	5.00
296	0	2.75-11	0.07	675	5.75
309	0	11-33	0.07	675	3.40
310	6.0	11-33	0.07	675	3.40
312	6.0	5.5-33	0.07	580-675	6.00
367B	6.0	2.2-33	0.07	675	1.67

Table.3.2. Growth conditions for $Al_xGa_{1-x}As$ specimens used in this study.

Samples	AlAs Fraction (%)	Dopant Impurity	Growth Technique	[V]/[III] Ratio	Growth Rate (μm/min.)	Growth Temp. (°C)
OM-2- 541A	30	Si	MOCVD	20	0.08	650
OM-2- 544A	30	undoped	MOCVD	20	0.08	650
OM-2- 556A	30	undoped	MOCVD	20	0.08	750
OM-2- 581A	35	undoped	MOCVD	20	0.08	650
OM-2- 583A	35	undoped	MOCVD	20	0.08	700
OM-2- 584A	35	undoped	MOCVD	20	0.08	750
OM-2- 585A	35	undoped	MOCVD	20	0.08	800
Y-015B	30	Be	LPE	-	-	800
Y-015C	30	Ge	LPE	-	-	800
-	20	Sn	LPE	-	-	-
-	30	Sn	LPE	-	-	-

region of a p-n junction diode or a Schottky barrier diode. For a good p-n diode with no surface leakage, the total current is composed of the diffusion current in the quasi-neutral region (QNR). When bulk diffusion current component dominates, the current expression is given by

$$I_f = I_d[\exp(V_a/V_t) - 1] \tag{3.1}$$

where V_a is the applied voltage; $V_T = kT/q$, and I_d is the magnitude of the saturation diffusion current.

$$I_d = q\, n_i^2 A\, [(D_n/L_n N_a) + (D_p/L_p N_d)] \tag{3.2}$$

where n_i is the intrinsic carrier density; A is the diode area; D_n (D_p) is the diffusion constant for electrons (holes); L_n (L_p) is the diffusion length for the electrons (holes), and N_a (N_d) is the acceptor (donor) density. If bulk generation-recombination current dominates, then the current is expressed by

$$I_r = I_{rg} \exp(V_a/2V_T) \tag{3.3}$$

where I_{rg} is the magnitude of generation-recombination current.

$$I_{rg} = q\, n_i W/2\tau_e \tag{3.4}$$

In Eqn.(3.4), W denotes the depletion layer width; $\tau_e = (\tau_n \tau_p)^{1/2}$ is the effective carrier lifetime in the space charge region; τ_n (τ_p) is the lifetime of electrons (holes), defined by

$$\tau_n = 1/(N_t\, \sigma_n \langle v_{th} \rangle) \tag{3.5}$$

where N_t is the trap density; σ_n (σ_p) is the capture cross section for electrons (holes); $\langle v_{th} \rangle$ is the average thermal velocity.

The total current can be expressed by

$$I_t = I_f + I_r = I_o \exp(V_a/nkT) \qquad (3.6)$$

where I_o is the saturation current; n is the ideality factor of a p-n junction diode which is usually used to identify the dominant current component in a p-n diode. Inspection of Eqns.(3.1) and (3.3) shows that the bulk diffusion current depends more strongly on temperature than the recombination current in the SCR. Since the recombination current in the SCR is inversely proportional to the effective carrier lifetimes (and hence directly related to the defect density in the transition region), measurements of I-V characteristics under forward bias condition would allow one to determine the effective lifetimes of a given material.

3.3. Capacitance-Voltage Measurement

The capacitance-voltage measurement can be used to determine the background doping concentration in the n- or p-type material using a Schottky barrier structure or a one sided abrupt p^+-n (or n^+-p) junction. The depletion capacitance across the Schottky barrier diode is given by

$$C(V_r) = \varepsilon_s A/W = A\{q\, \varepsilon_s N_d/[2(\phi_j + V_r - kT/q)]\}^{1/2} \qquad (3.7)$$

where ε_s is the dielectric constant of given material; ϕ_j is the built-in potential, and V_r is the applied reverse voltage. Eqn.(3.7)

shows that the depletion capacitance of a Schottky diode is proportional to the square root of dopant concentration and inversely proportional to the square root of the applied voltage. If the inverse of the capacitance square (C^{-2}) is plotted as a function of the reverse bias voltage V_r, then the background concentration can be calculated from the slope of C^{-2} versus V_r using the following expression

$$C^{-2}(V_r) = [2/(q\ _sA^2N_d)](\Phi_j + V_r) \qquad (3.8)$$

The intercept of C^{-2} versus V_r plot in the voltage axis yields values of Φ_j which is related to the barrier height of a Schottky diode by

$$\Phi_{Bn} = \Phi_j + V_n + kT/q - \Delta\Phi_i \qquad (3.9)$$

where

$$V_n = E_c - (kT/q)\ln(N_d/N_c) \qquad (3.10)$$

and $\Delta\Phi_i$ is the image lowering potential of a Schottky diode; N_c is the effective density of states in the conduction band.

3.4. A.C. Admittance Measurement

By measuring the conductance and susceptance as a function of frequency, one can evaluate each component of the equivalent circuit of a p-n junction diode [30]. It can be shown that in the frequency range from 0.11 to 700 MHz, a p-n junction diode can be described by a discrete 3 element circuit consisting of a series resistance R_s, a parallel resistance R_p and a junction capacitance C. The impedance of

the equivalent circuit is given by

$$Z(w) = R_s + [R_p/jwC]/[R_p + 1/jwC]$$
$$= Z_1(w) + Z_2(w) \qquad (3.11)$$

where

$$Z_1(w) = R_s + R_p/[1+(wR_pC)^2] \qquad (3.12)$$

$$Z_2(w) = wR_pC/[1+(wR_pC)^2] \qquad (3.13)$$

Then, the admittance is given by

$$Y(w) = 1/Z(w) = Z_1/(Z_1^2 + Z_2^2) + j[Z_2/(Z_1^2 + Z_2^2)] \qquad (3.14)$$

In the low and high frequency limits, the imaginary part of Y(w) diminishes and the real part becomes

$$w \to 0, \quad Re\{Y(w)\} = 1/(R_p + R_s) \qquad (3.15)$$

$$w \to \infty, \quad Re\{Y(w)\} = 1/R_s \qquad (3.16)$$

Therefore, once the series resistance and the parallel resistance are determined, the junction capacitance can be calculated from a plot of Im{Y(w)} versus Re{(Y(w)} for a given frequency.

3.5. Thermally Stimulated Capacitance Measurement

The TSCAP experiment [31] is carried out by first reverse biasing a p-n junction diode or a Schottky diode, and then the diode is cooled down to liquid nitrogen temperature (77K). After temperature reaches 77K, the diode is momentarily zero biased to fill the majority carrier

traps and returned to reverse bias condition, and the temperature is then raised from 77 to 400K. The thermal scan of capacitance versus temperature plot is then taken by using an X-Y recorder. A capacitance step is observed from the C versus T plot if majority or minority carrier emission is taking place in the trap within a certain temperature range. The amplitude of this capacitance step is directly proportional to the trap density, which is expressed as

$$N_t = N_d(2\Delta C/C_o) \qquad (3.17)$$

where C_o is the depletion layer capacitance and ΔC is the capacitance change due to the majority or minority carrier emission. Thus, knowing N_d (or N_a) and C_o at the temperature where the capacitance step was observed, the trap density can be calculated from Eqn.(3.17). Note that Eqn.(3.17) is valid only for the case when N_t is less than 0.1 N_d. For the case of large trap density, a more exact expression should be used instead.

3.6. Deep Level Transient Spectroscopy Measurement

The Deep Level Transient Spectroscopy (DLTS) experiment is a high frequency (f > 1 MHz) transient capacitance technique, which was introduced first by Lang in 1974 [32]. The DLTS scan displays the spectrum of deep level traps in the forbidden gap of a semiconductor as positive or negative peaks on a flat baseline as a function of temperature. Although this kind of measurement is time consuming, it offers several advantages such as sensitive, easy to analyze and capable of measuring the traps over a wide range of depth in the

forbidden gap. By properly changing the experimental conditions, one can measure the following parameters

(a) Minority and majority carrier traps.

(b) Activation energy of each defect level.

(c) Defect concentration which is directly proportional to peak height.

(d) Defect concentration profile.

(e) Emission and capture cross sections of electron and hole.

3.6.1. Principles of the DLTS Measurement

The capacitance transient is associated with the return to thermal equilibrium of the carrier occupancy in a trap level following an initial nonequilibrium condition. The polarity of the DLTS peak depends on the capacitance change after trapping the minority or majority carriers. Because an increase in trapped minority carriers in the SCR would result in an increase in the junction capacitance, the trapping of minority carriers will produce a positive polarity peak, and vice verse. For example, in a p^+-n junction diode, the SCR extends mainly into the n-type region, and the local charges are due to positively charged ionized donors. If a forward bias is applied, the minority carriers (holes) will be injected into this region. Once the holes are trapped in a defect level, the net positive charges in such region will increase. This results in a narrow SCR width which implies a positive capacitance change. Thus, the DLTS signal will have a positive peak. Similarily, if the majority carriers are injected into this region and captured by the majority carrier traps, which reduce

the local charges, the SCR width will be wider, implying a decrease of the junction capacitance. Therefore, the majority carrier trapping will result in a negative DLTS peak.

3.6.2. Defect Concentration

The defect concentration is directly proportional to the peak height as described before, and the peak height is proportional to the capacitance change C(Ø). Therefore, the defect concentration N_t is proportional to C(Ø) which can be derived as follows: Let C(t) be the capacitance transient, which is proportional to the electron (holes) emitted to the conduction (valence) band, then

$$C(t) = A\{q\,\varepsilon_s[N_d - N_t\exp(-t/\tau)] \;/\; [2(\Phi_j + V_r + kT/q)]\}^{1/2}$$
$$= C_o\{1 - [N_t\exp(-t/\tau)/N_d]\}^{1/2} \qquad (3.18)$$

where t is time; τ is the carrier emission time constant; $C_o = C(V_r)$ is the junction capacitance at the quiescent reverse bias condition. Using binomial expansion and the condition that $N_t/N_d \ll 1$, Eqn.(3.18) reduces to a simple form as

$$C(t) = C_o[1 - N_t\exp(-t/\tau)\,2N_d] \qquad (3.19)$$

Equation (3.19) can be rewritten as

$$N_t\exp(-t/\tau) = (2\,\Delta C(t)/C_o)\,N_d \qquad (3.20)$$

where $\Delta C(t) = C_o - C(t)$. After determination of C(Ø) from the DLTS measurement, the defect concentration N_t can be calculated from the Eqn.(3.20) by setting t=Ø. However, for the case when the defect

concentration is comparable or higher than the free carrier concentration, Eqn.(3.2Ø) is not applicable, because of its oversimplification. Instead, one must use the following expression [33]

$$N_t = \frac{2\,\Delta C \times C(\infty) - \Delta C^2}{C^2(\infty)} \times (N_d - N_a + N_t) \qquad (3.21)$$

where $\Delta C = C(\infty) - C(Ø)$ and $N_d - N_a + N_t$ is the net donor or acceptor concentration including the ionized traps. For small N_t and $C \ll C(\infty)$ Eqn.(3.21) reduces to Eqn.(3.2Ø) by neglecting ΔC^2.

3.6.3. Activation Energy of the Defect Level

The decay time constant in the capacitance transient during the DLTS experiment is associated with specific time constant which is equal to the reciprocal of the emission rate. For an electron trap, the emission rate e_n is a function of temperature, capture coefficient and activation energy, and can be expressed by [34]

$$e_n = (\sigma_n \langle V_{th} \rangle N_c / g) \exp[(E_c - E_t)/kT] \qquad (3.22)$$

where E_t is the activation energy of the trap, g is the degeneracy factor, σ_n is the electron capture cross section which is dependent on temperature, and is given by

$$\sigma_n = \sigma_\infty \exp(-\Delta E_b/kT) \qquad (3.23)$$

where σ_∞ is the capture cross section at very high temperature, ΔE_b is the barrier height of the capture cross section for the trap. e_n

can be written as

$$e_n = B\,T^2 \exp\{[E_c - (E_t + \Delta E_b)]/kT\}$$
$$= B\,T^2 \exp[(E_c - E_m)/kT] \qquad (3.24)$$

where B is the proportionality constant, which is independent of temperature. From this relation, e_n increases with increasing the temperature. The capacitance transient is rearranged from Equation (3.19) as

$$C(t) = C_o(N_t/2N_d)\,\exp(-t/\tau)$$
$$= \Delta C(\emptyset)\,\exp(-t/\tau) \qquad (3.25)$$

where $\tau = e_n^{-1}$ is the reciprocal emission time constant.

The procedure for determining the activation energy of a defect level in a semiconductor is described as follows. First, set t_1 and t_2 in a dual gated boxcar integrator, then

$$C(t_1) = C(\emptyset)\,\exp(-t_1/\tau) \qquad (3.26)$$

$$C(t_2) = C(\emptyset)\,\exp(-t_2/\tau) \qquad (3.27)$$

The DLTS scan along the temperature axis is obtained by taking the difference of Eqn.(3.26) and (3.27), which yields

$$s(\tau) = C(\emptyset)[\exp(-t_1/\tau) - \exp(t_2/\tau)] \qquad (3.28)$$

The maximum emission rate, τ_{max}^{-1} is obtained by differentiating $s(\tau)$ with respect to τ, and setting $ds(\tau)/d\tau = \emptyset$, which yields

$$\tau_{max} = (t_1 - t_2) \,/\, \ln(t_1/t_2) \qquad (3.29)$$

Under this condition, $s(\tau)$ reaches its maximum value at a specific temperature. The emission rate is given by $e_n=1/\tau_{max}$ for each t_1 and t_2 setting. By changing t_1 and t_2 several times, a set of temperatures corresponding to this set of τ_{max} (emission rate e_n) can be obtained as is shown in Fig.3.1. The activation energy of the trap can be calculated from the slope of the Arrhenius plot.

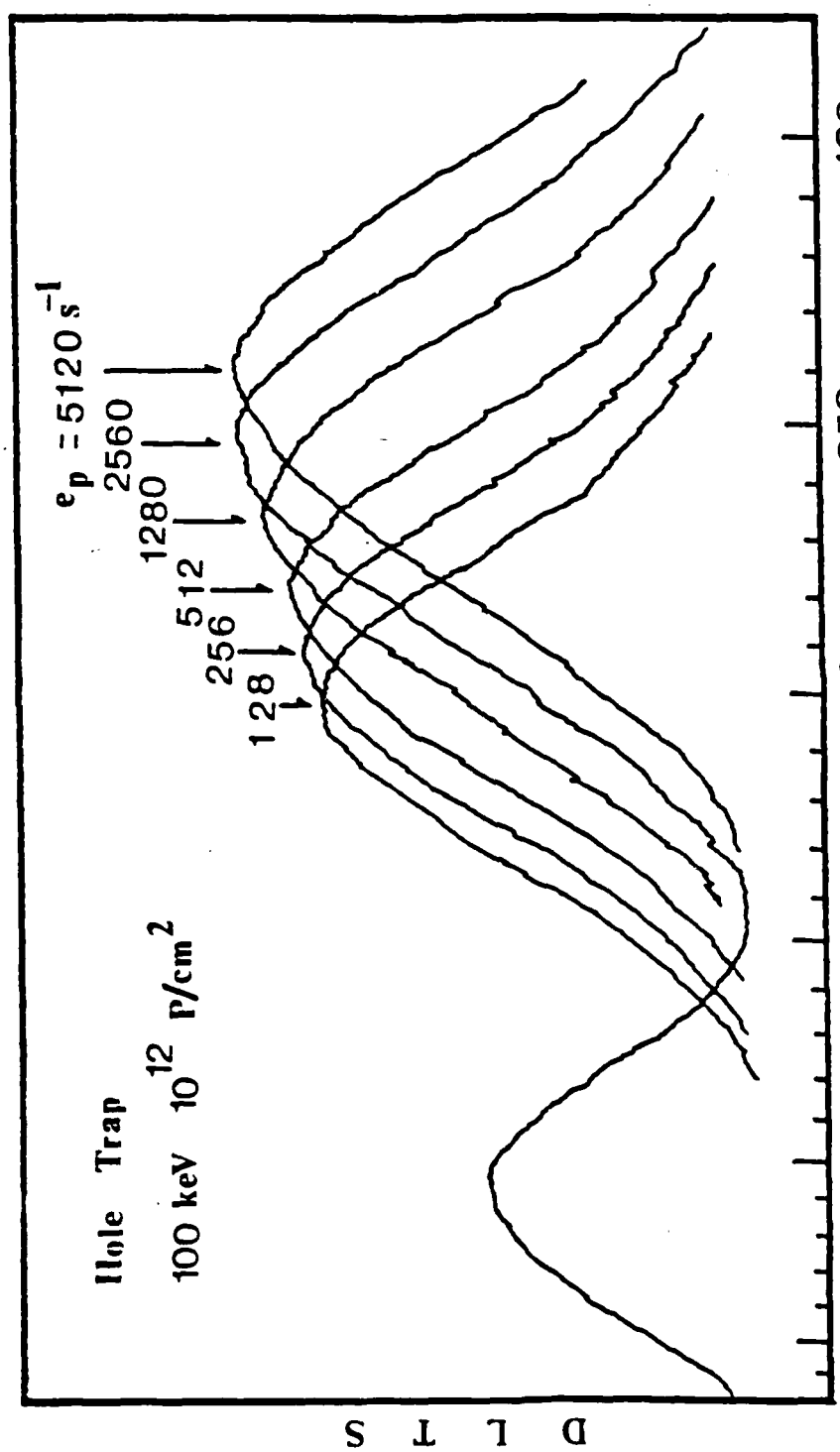

Fig.3.1 DLTS scans of hole traps in proton irradiated GaAs for different window rates.

CHAPTER IV
THEORETICAL TREATMENTS OF DEFECTS IN GALLIUM ARSENIDE AND ALUMINUM GALLIUM ARSENIDE

The grown-in defects in GaAs and $Al_xGa_{1-x}As$ commonly exhibit various characteristics depending on the growth technique and the growth condition. And, many experimental methods for studying the deep-level defects are based on the thermal emission of carriers from the traps within the depletion region of a diode. However, due to the non-uniformity of electric field in that region, the electric-field enhanced emission rate yields a non-exponential capacitance transients. Furthermore, for $Al_xGa_{1-x}As$, hydrostatic pressure or incorporation of aluminum atoms changes the position of conduction band minima, which results in more complicated carrier emission and capture transition associated with each conduction minimum and trap.

Therefore, to identify the most probable physical origins of the EL2 center in GaAs and the DX center in $Al_xGa_{1-x}As$, the following subjects were carried out in this study:

(1) The thermal kinetic reactions in three different kinetic processes for MOCVD and VPE grown GaAs (section 4.1.1 through 4.1.3).

(2) The electric-field enhanced thermal emission rates with four different types of potential well for the EL2 center in MOCVD grown GaAs (section 4.1.4).

(3) The electron emission and capture transition associated with three conduction band minima for the DX center in MOCVD and LPE grown $Al_xGa_{1-x}As$ (section 4.2.1 and 4.2.2).

(4) The electric-field enhanced thermal emission rates with Coulombic and Yukawa potential well for the DX center in MOCVD and LPE grown $Al_xGa_{1-x}As$ (section 4.2.3).

4.1. EL2 Center in Gallium Arsenide

In order to predict the physical origins of the EL2 center and the dependence of its density on [As]/[Ga] mole fraction ratio for the MOCVD and VPE grown GaAs, three different kinetic processes will be considered [40]. In the growth process, vacancies, interstitials, and the antisites are likely to form at high temperature under thermal equilibrium condition. In the cooling process, Ga-vacancies may pair with As_i or As_{As}, or the four nearest As_{As} may cling to As_{Ga} to form the EL2a or EL2b electron trap. In the annealing process, the EL2b level may be annihilated, while the EL2a level is created for $T > 500\ ^{o}C$. Finally, to determine the charge state of the EL2 center, the electric field dependent emission rate of trapped charge is studied for the different types of potential well; namely, the Coulombic well which has a positive charge state when empty, the Dirac well, square well, polarization well and dipole well which all have a neutral charge state from different physical origins.

4.1.1. Growth process

In the growth process, we will consider the defect formation under thermal equilibrium only for the As-rich

condition (i.e., r>1, where r is defined by Eqn.(4.1)).

(a) MOCVD grown GaAs epitaxial material

In MOCVD grown GaAs, we will consider the case in which arsine (AsH_3) and trimethylgallium (TMGa) are used as sources for As and Ga, respectively. If the initial mole fraction ratio of arsine to TMGa is equal to r, then

$$[AsH_3]/[Ga(CH_3)_3] = r \qquad (4.1)$$

where the square bracket in Eqn.(4.1) represents the mole fraction of arsine and TMGa gas. During the crystal growth, arsine will decompose into either $As_4(g)$ or $As_2(g)$, depending on the growth temperature. In general, arsine will decompose into $As_4(g)$ during the epitaxial growth if the growth temperature is below 1000 ^oC, whereas arsine will decompose into $As_2(g)$ in the melt growth if the growth temperature is above 1400 ^oC. The growth temperature for the MOCVD process is usually below 1000 ^oC, and thus the reaction of arsine can be written as

$$AsH_3(g) = (1/4)As_4(g) + 3/2\ H_2(g) \qquad (4.2)$$

The chemical reaction equation of $As_4(g)$ and TMGa can be described by

$$Ga(CH_3)_3 + (1/4)As_4(g) + (3/2)H_2(g)$$
$$= GaAs(s) + 3CH_4(g) \qquad (4.3)$$

During the deposition, the formation of native defects may be explained by the following reactions under As-rich condition

$$(1/4)As_4(g) = As_{As}(s) + V_{Ga} \quad (4.4)$$

$$(1/4)As_4(g) = As_i \quad (4.5)$$

$$(1/2)As_4(g) = As_{As}(s) + As_{Ga} \quad (4.6)$$

Using the law of mass action in Eqns.(4.4) through (4.6), the concentration of V_{Ga}, As_i, and As_{Ga} can be expressed, respectively, by

$$[V_{Ga}] = k_1' r^{1/4} \quad (4.7)$$

$$[As_i] = k_2' r^{1/4} \quad (4.8)$$

$$[As_{Ga}] = k_3' r^{1/2} \quad (4.9)$$

(b) VPE grown GaAs epitaxial material

In the VPE grown GaAs, if arsine (AsH_3) and gallium chloride (GaCl) were used as sources for As and Ga, respectively, then the initial mole fraction ratio of arsine and gallium chloride can be expressed by

$$[AsH_3]/[GaCl] = r \quad (4.10)$$

The reaction of $As_4(g)$ and GaCl can be expressed by

$$GaCl + (1/4)As_4(g) + (1/2)H_2(g) = GaAs(s) + HCl(g) \quad (4.11)$$

During the deposition, As atom will be deposited on As sites, As interstitial sites or Ga sites according to Eqns.(4.4) to (4.6). Thus, the concentration of V_{Ga}, As_i, and As_{Ga} can be expressed by

$$[V_{Ga}] = k_4' r^{1/4} \tag{4.12}$$

$$[As_i] = k_5' r^{1/4} \tag{4.13}$$

$$[As_{Ga}] = k_6' r^{1/2} \tag{4.14}$$

From Eqns.(4.7) to (4.9) and (4.12) to (4.14), it is noted that for the MOCVD and VPE grown GaAs, the density of both V_{Ga} and As_i defect varies with $r^{1/4}$, whereas the density of As antisite defect is proportional to $r^{1/2}$ during the growth process.

4.1.2. Cooling process

During the post growth cooling process, formation of the most probable native defects for the EL2 center can be explained via the kinetic reaction equations given as follows. The As antisite defect [9,10] can be formed from V_{Ga} and As_i, which is written as

$$As_i + V_{Ga} = As_{Ga} \tag{4.15}$$

The As_{Ga}-As_4 defect cluster [236] may be created when As_{Ga} pairs with its four nearest As_{As}, which is expressed by

$$As_{Ga} + 4As_{As} = As_{Ga}\text{-}As_4 \tag{4.16}$$

The As_{Ga}-V_{As} defect complex [11,35] may be formed by V_{Ga} pairing with its neighbor As_{As}, and is given by

$$As_{As} + V_{Ga} = As_{Ga}\text{-}V_{As} \tag{4.17}$$

Using the law of mass action in the reaction equations given above, the As_{Ga}, As_{Ga}-As_4 and As_{Ga}-V_{As} defect concentration can be expressed,

respectively, by

$$[As_{Ga}] = K_a [As_i] [V_{Ga}] = K_a'' r^{1/2} \quad (4.18)$$

$$[As_{Ga}\text{-}As_4] = K_b [As_{Ga}] = K_b'' r^{1/2} \quad (4.19)$$

$$[As_{Ga}\text{-}V_{As}] = K_c [V_{Ga}] = K_c'' r^{1/4} \quad (4.20)$$

Equations (4.18) and (4.19) predict that the concentration of $[As_{Ga}]$ antisite defect and $[As_{Ga}\text{-}As_4]$ defect cluster is proportional to $r^{1/2}$, while Eqn.(4.20) shows that the concentration of $[As_{Ga}\text{-}V_{As}]$ antisite complex varies with $r^{1/4}$.

Figure 4.1 shows the plot of EL2a and EL2b trap density as a function of [As]/[Ga] mole fraction ratio calculated from Eqns.(4.18) through (4.20) along with the published data [3,11] and our experimental data for the MOCVD grown GaAs. results show that for As-rich condition, the EL2a trap may be attributed to the As_{Ga} antisite defect or the $As_{Ga}\text{-}As_4$ complex with its concentration being proportional to $r^{1/2}$. On the other hand, the EL2b trap may be ascribed to the As antisite plus As vacancy complex with its concentration being varied with $r^{1/4}$. This prediction is consistent with the experimental observation for the MOCVD grown GaAs [37].

4.1.3. Annealing Process

The EL2a level may be formed from the EL2b level via high temperature thermal annealing. This is due to the fact that EL2b trap may gain sufficient thermal energy during high temperature annealing, and then decomposes into V_{Ga} and As_{As} according to the inverse

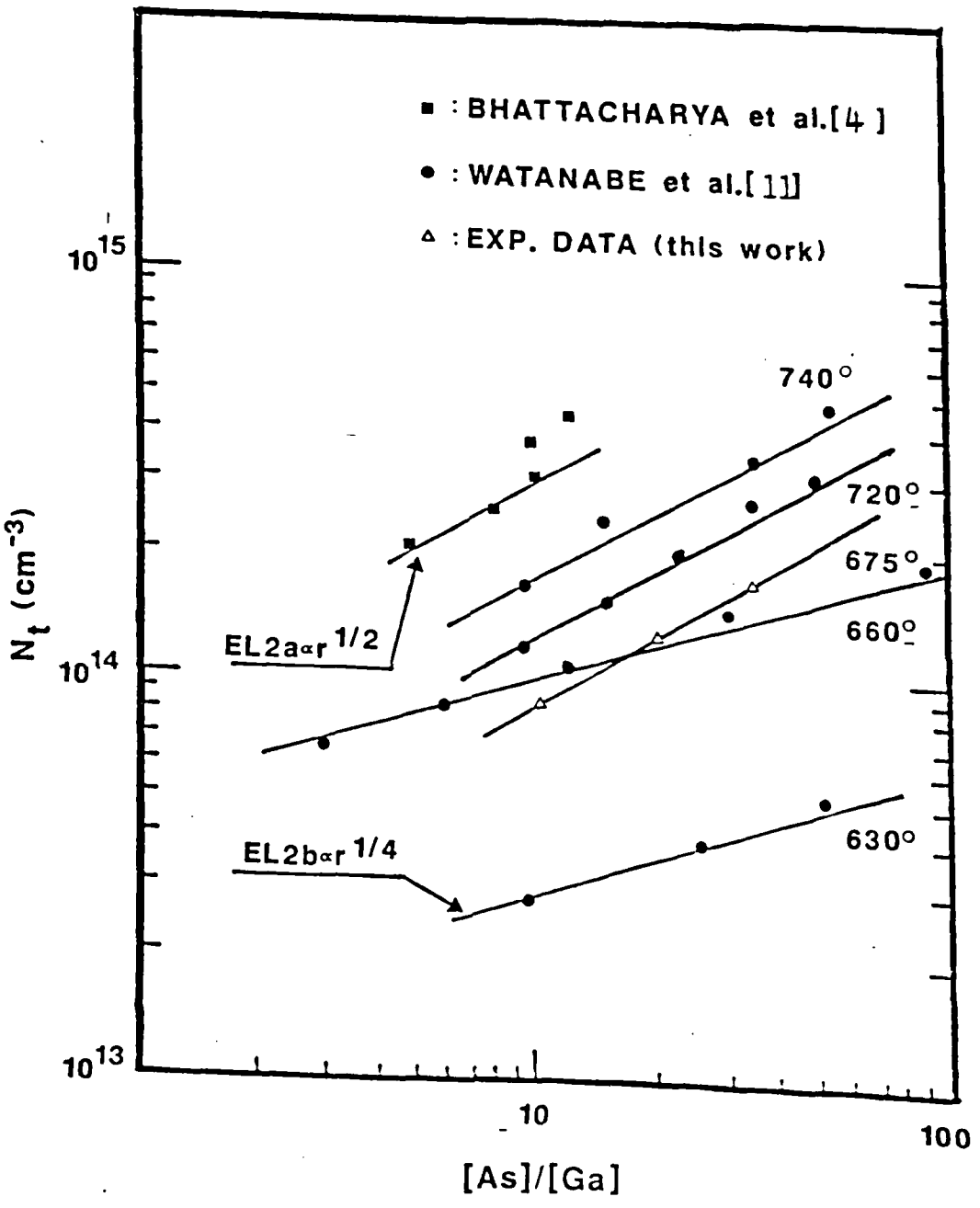

Figure 4.1 Theoretical calculations and experimental data of the concentration of EL2a and EL2b electron traps vs [As]/[Ga] mole fraction ratio as compared to the published data for GaAs.

reaction of Eqn.(4.17) if the annealing temperature is higher than 500 ^{o}C. An As_{Ga} antisite defect will be formed when a V_{Ga} pairs with the As_i site, according to Eqn.(4.15). This is supported by the experimental data of Taniguchi et al.[38] and Day et al.[39], which showed the outdiffusion of one of the host atoms, probably Ga, resulting in a vacancy or vacancy complex observed in the MBE and LEC grown GaAs materials.

4.1.4. Potential Well

As discussed above, the most probable physical origin for the EL2a electron trap may be ascribed to the As_{Ga} defect or As_{Ga}-As_4 cluster, and the physical origin of EL2b trap is attributed to the As_{Ga}-V_{As} complex. The charge state for these two electron traps may be unveiled if the type of potential well for each of these two traps is known. This can be obtained by analyzing the electric field enhanced emission rates deduced from the nonexponential DLTS spectra for the EL2 electron trap. Table 4.1 [40] summarizes four different electric field enhanced emission rates by taking into account the three-dimensional Poole-Frenkel effect and phonon-assisted tunneling effect. For example, the electric field enhanced emission rates for the Coulombic potential well can be expressed by [41]

$$e_{nHC}/e_{no} = \{[\int_o^{2\pi}\int_o^{\pi/2} \sin(\theta)\exp(\Delta E_{ti}/kT)d\theta\, d\phi + \int_o^{2\pi}\int_o^{\pi/2} \sin(\theta)\, d\theta\, d\phi\,]/4\pi\} + \int_o^{(E_{ti}-\Delta E_{ti})/kT} \exp\{z - z^{3/2}[4(2m^*)^{1/2}(kT)^{3/2}/3q\hbar F]$$

$$x\ [1-\ (\Delta E_{ti}/zkT)^{5/3}]\}\ dz \qquad (4.21)$$

where e_{no} is the emission rate at zero electric field. ΔE_{ti} is the Poole-Frenkel barrier lowering due to the external electric field. $\Delta E_{ti} = q[qF\cos(\theta)/\varepsilon_o\varepsilon_s]^{1/2}$, and F is the applied electric field. The first term in Eqn.(4.21) is due to the three-dimensional Poole-Frenkel effect, and the second term is due to the phonon-assisted tunneling effect. Since the electric field varies with position within the depletion region of a reverse biased p-n junction, the emission rates are not constant within the depletion region. The DLTS spectrum due to the field dependent emission rates can be expressed by

$$S(\tau) = \Sigma \exp(-e_{ni}t_1) - \Sigma \exp(-e_{ni}t_2) \qquad (4.22)$$

Figure 4.2 shows the calculated enhanced emission rates versus electric field for the EL2a electron trap in GaAs, for four different types of potential well (i.e., Coulombic well, dipole well, Dirac well, and polarization well). The results show that even though the various potential wells exhibit quite different electric field enhanced emission rates, determination of the type of potential well for the EL2 level in GaAs is still far from clear. This may be due to the fact that the electric field in the defect potential well is strongly anisotropic. Furthermore, the theoretical calculations for the electric field enhanced emission rates are based on continuum built-in electric field in the depletion region, which is not appropriate for a real case.

Table 4.1. Electric field enhanced emission rates for four different types of potential well.

Potential Well	R	3-Dim. Poole-Frenkel Effect	Phonon-Assisted Tunneling Effect
Coulombic	$\Delta E_{ti}/kT$	$[(R-1)\exp(R)+1]/R^2+1/2$	$\int_0^{(E_{ti}-\Delta E_{ti})/kT} \exp\{z-z^{3/2}[4(2m^*)^{1/2}(kT)^{3/2}/3q\hbar F] \times [1-(\Delta E_{ti}/zkT)^{5/3}]\}dz$
Square	$\Delta E_{ti}/kT$	$[\exp(R)-1]/(2R)+1/2$	$\int_0^{(E_{ti}-\Delta E_{ti})/kT} \exp\{z-z^{3/2}[4(2m^*)^{1/2}(kT)^{3/2}/3q\hbar F] \times [1-(qFr_o/zkT)^{3/2}]\}dz$
Polarization	$\Delta E_{ti}/kT$	$1/2+(5/8)\int_0^1 Rt^{1/4}\cosh(Rt)dt$	$\int_0^{(E_{ti}-\Delta E_{ti})/kT} \exp\{z-[(8m^*)^{1/2}/\hbar] \times (-A_1/R^4-qFx+zkT)^{1/2}dx\}dz$
Dirac	0	0	$\int_0^{E_{ti}/kT} \exp\{z-z^{3/2}[4(2m^*)^{1/2}(kT)^{3/2}/3q\hbar F]\}dz$

where E_{ti} : ionization energy of the trap
$\Delta E_{ti}/q$: lowering of potential barrier
F : applied electric field
r_o : radius of trap potential well

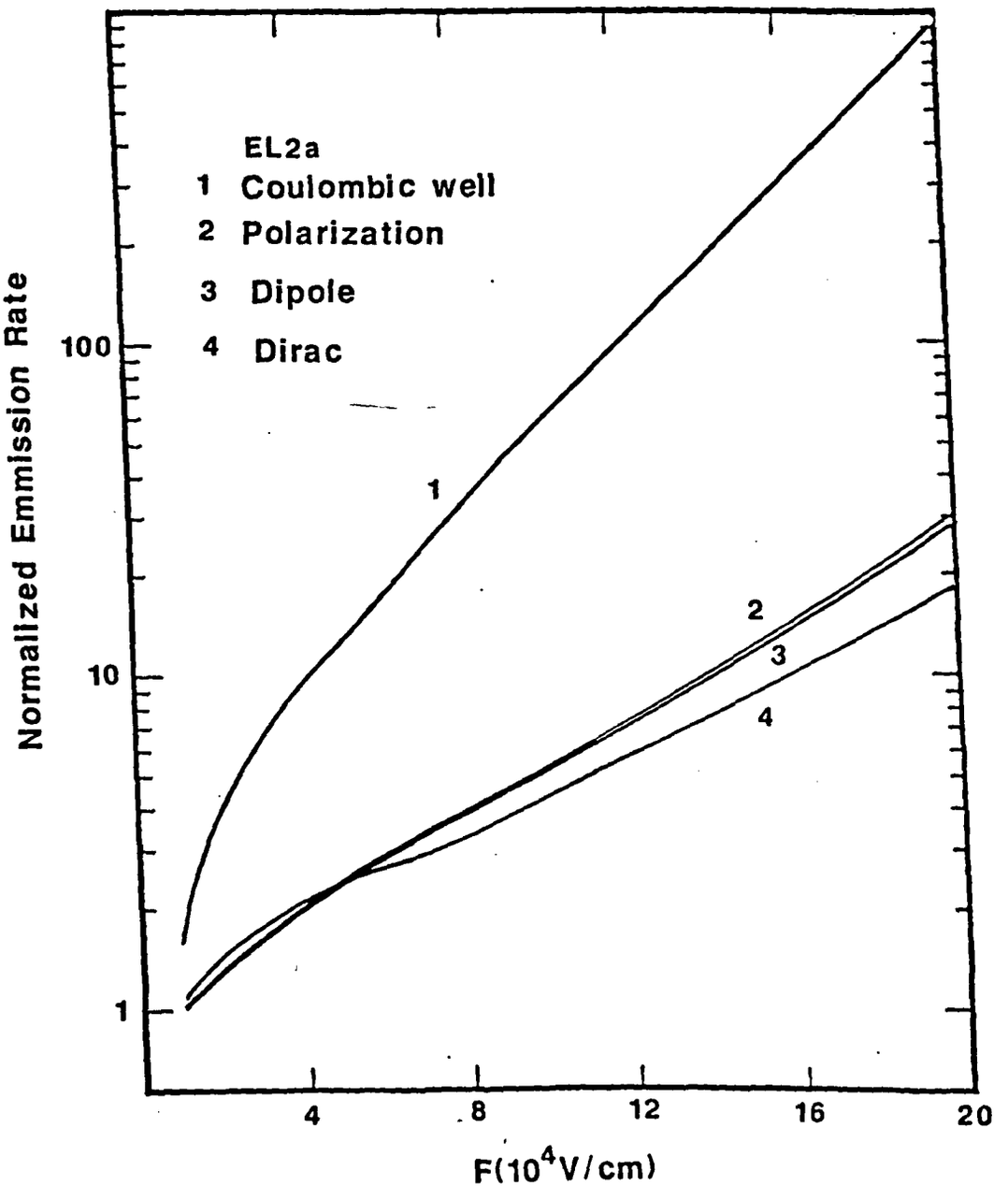

Figure 4.2 Normalized electron emission rates vs electric field for the EL2a electron trap, assuming Coulombic well(1), polarization well(2), dipole well(3), and Dirac well(4).

4.2. DX center in Aluminum Gallium Arsenide

In AlGaAs, it is known that the shift in the conduction band minima, namely Γ, L and X, caused by substitution of aluminum atoms into gallium sublattices, makes the electrical and optical properties of that system strongly dependent on the aluminum composition. Consequently, in order to identify the nature of the DX center, it is necessary to correlate the electron emission (capture) from the trap center to the conduction band structure.

4.2.1. Electron Emission and Capture

It is well established that, for $Al_xGa_{1-x}As$, the LΓ intervalley energy $E_{L\Gamma}$ in the conduction band changes with Al alloy composition or the hydrostatic pressure. In order to identify the natures of electron emission and capture with respect to the conduction band minima, let us correlate the DLTS experiment and the capacitance measurement performed at low temperature.

In a typical DLTS experiment, the electron thermal emission rate e_n from a trap level to the non-spherical conduction band minima can be written as (Eqn.(3.24))

$$e_n = B\, T^2 \exp\{[E_c - (E_{t1} + \Delta E_b)]/kT\} \qquad (4.23)$$

$$B = 3.26\times10^{21} g_n\, \sigma^e [(m_d^*/m_o)^{2/3}/(m_c^*/m_o)^{1/2}] \exp(\alpha/k) \qquad (4.24)$$

where $E_{t1} = E_t^o - \alpha T$ is the activation energy of the trap; α is the temperature coefficient; $\sigma^e = \sigma_\infty^e \exp(-\Delta E_b/kT)$ is the thermally activated emission cross section with barrier energy ΔE_b; g_n is the degeneracy factor; m_d^* and m_c^* are the effective masses for the

density of states and conductivity, respectively. From the Arrhenius plot of Eqn.(4.23), one can determine the values of $[E_c-(E_{t1}+\Delta E_b)]$ and B. Again, one can determine the values of each argument of the exponential term in Eqn.(4.23) separately using the temperature dependent electron capture cross section, which also results from the same DLTS spectra as follows:

A series of DLTS peaks at a given temperature can be obtained by varying the trap filling time t_c, which yields the saturated peak $\Delta C(\infty)$ at a large value of t_c. Then the electron capture constant c is expressed by [31]

$$1 - \frac{\Delta C(t_c)}{\Delta C(\infty)} = \exp(-ct_c) \qquad (4.24)$$

From the temperature dependent capture rates measured by changing the peak temperature of the DLTS spectrum, one can determine the energy barrier for electron capture by the following equations.

$$c = \sigma_c \langle v_{th} \rangle n_o \qquad (4.25)$$

$$\sigma_c = \sigma^{\infty} \exp(-\Delta E_b/kT) \qquad (4.26)$$

Now, in order to determine the defect parameters by capacitance-voltage measurement performed in low temperature (100 K) range, let us consider the one dimensional band diagram for the reverse biased n-type Schottky barrier structure. The quasi-Fermi level E_f intercepts the trap level E_t (measured from the Γ minimum) at a distance d from the metal-semiconductor interface at x=0. If the depletion

region is divided into two regions, then in thermal equilibrium, the trap is empty for $0<x<d$, and is occupied for $d<x<W$. This is true if the shallow donor impurities in the delpetion region are fully ionized in the depletion region. Thus, the total density of ionized char es is $N_d+ N_t$ for $0<x<d$ and N_d for $d<x<W$. Now, let the band bending energy at $x=d$ be qV_L, which is independent of bias, then the ionization energy of deep-level defect center is [42]

$$E_{t2} = q\, V_L + E_f \tag{4.27}$$

Integrating the Poisson's equation yields the excess voltage V_e associated with the trap density N_t for $0<x<d$ as

$$V_e^{1/2} = A\ (\varepsilon q\, N_t/2)^{1/2}\ (C_w^{-1} - C_L^{-1}) \tag{4.28}$$

where $C_w=\varepsilon\, A/W$ is the measured diode capacitance, $C_L=\varepsilon\, A/L$, and A is the diode area. V_e can be determined from a set of C-V measurements performed when the traps are full for $0<x<W$ and empty for $0<x<d$. If $C_s(V)$ represents the depletion layer capacitance when the trap is filled with electrons for $0<x<W$, then

$$V_L = C_L^{-2}(dV/dC_s^{-2}) \tag{4.29}$$

According to Eqn.(4.28), a plot of $V_e^{-1/2}$ versus C_w^{-1} yields accurate values of C_L and N_t. Finally, Eqn.(4.27) gives the activation energy of deep-level defect at the measurement temperature.

A comparison of the activation energies obtained by both C-V (E_{t2}) and DLTS measurements (E_{t1}) shows a considerable difference between these two data. This indicates that the final states of the

emission transition cannot be in the Γ minimum which is the lowest conduction band for the Al composition up to 40 %. Instead, it has been shown that the electron emission transition from the DX center is associated with L minimum [18]. Thus, the energy difference between the Γ and L conduction band minima and the ionization energy of shallow donor impurity associated with each conduction band minimum can be used to identify the nature of DX center in $Al_xGa_{1-x}As$. This is discussed next.

4.2.2. Ionization Energy of Donor Impurity Associated with Conduction Band

The measurement of Hall coefficient as a function of Al composition and hydrostatic pressure enables us to determine the activation energy of shallow donor level associated with each conduction band minimum in $Al_xGa_{1-x}As$. For the electron distribution involving all three conduction minima (Γ, L, and X), the Hall coefficient R_H is expressed as

$$R_H = \frac{1}{en} \left\{ \frac{\alpha_\Gamma + (\mu_{HL}/\mu_{H\Gamma})^2 \alpha_L + (\mu_{HX}/\mu_{H\Gamma})^2 \alpha_X}{[\alpha_\Gamma + (\mu_{HL}/\mu_{H\Gamma}) \alpha_L + (\mu_{HX}/\mu_{H\Gamma}) \alpha_X]^2} \right\}$$

$$= R^*_H/en \qquad (4.30)$$

where, $\alpha_i = n_i/n$ (i= Γ,L) is the fraction of the total number of electrons in a particular minimum and μ_{Hi} is the Hall mobility in this minimum. Equation (4.30) indicates that if more than one minimum is associated with the electron distribution, n is not simply equal to $1/R_He$, but rather to R^*_H/R_He. The density of electron in each

conduction band depends on the relative position of the band and temperature; and R^*_H is a function of pressure, composition and temperature.

Using Boltzmann statistics for the nondegenerate case and parameters given in table 4.2, R^*_H can be separated into a function of composition ratio and of pressure, respectively [44]. Then, the contribution of freeze-out effect to the Hall coefficient for each conduction minimum, that is, the value of activation energy E_d can be determined from the following equation provided that all electrons are resided either in Γ or in X conduction band minima.

$$\frac{n(P)}{n_o} = \frac{1+RN_a+[(1+RN_a)^2+4R(N_d-N_a)]^{1/2}}{1+R(P)N_a+[(1+R(P)N_a)^2+4R(P)(N_d-N_a)]^{1/2}} \qquad (4.31)$$

where $R = \exp(E_{do}/kT)/\beta N_{co}$, $R(P) = \exp(E_d(P)/kT)/\beta N_c(P)$, P is a hydrostatic pressure, N_a and N_d are acceptor and donor concentrations which are independent of pressure, N_c is the effective density of conduction band states which is dependent on temperature and pressure, and β is the impurity spin degeneracy. The donor ionization energies calculated from the lowest donor level to the lowest conduction band minimum as a function of pressure for the Sn doped AlGaAs are shown in Fig.4.3. Up to 9 Kbar, the donor level associated with Γ minimum is the lowest, while in the pressure range of 9 to 24 Kbar, the donor level associated with L minimum becomes the lowest. At pressure higher than 24 Kbar, the lowest donor level is associated with X minimum.

The donor ionization energy as a function of Al composition can be evaluated by using the temperature dependence of electron

Table 4.2. Electronic band parameters for $Al_xGa_{1-x}As$ [43].

Dependence	Parameter	$Al_xGa_{1-x}As$
ALUMINUM COMPOSITION	Bandgap Energy (eV)	$E_g^{\Gamma} = 1.424 + 1.247x \quad (0<x<0.45)$
		$1.656 + 0.215x + 1.147x^2 \quad (0.45<x<1)$
		$E_g^{L} = 1.708 + 0.642x$
		$E_g^{X} = 1.900 + 0.125x + 0.143x^2$
	Density of States Effective Mass	$M_e^{\Gamma} = 0.067 + 0.083x$
		$M_e^{L} = 0.56 + 0.1x$
		$M_e^{X} = 0.85 - 0.14x$
	Conductivity Effective Mass	$M_c^{\Gamma} = 0.067 + 0.083x$
		$M_c^{L} = 0.11 + 0.03x$
		$M_c^{X} = 0.32 - 0.06x$
HYDROSTATIC PRESSURE (10^{-6} eV/bar)	Bandgap Energy (eV)	$dE_g^{\Gamma}/dP = 11.5 - 1.3x$
		$dE_g^{L}/dP = 2.8$
		$dE_g^{X}/dP = -0.8$
TEMPERATURE (10^{-4} eV/K)	Bandgap Energy (eV)	$dE_g^{\Gamma}/dT = -3.95 - 1.15x$
		$dE_g^{X}/dT = -3.6$

concentration to the Boltzmann distribution factor for the each conduction band minima.

$$\exp(-E_d/kT) = n(N_a+n)/[(N_d-N_a)\ N_c] \qquad (4.32)$$

As can be shown in Fig.4.4, up to 25 % of Al content, the donor level associated with Γ minimum is the lowest, while in the range of 25 to 52 % of Al content, the one associated with L minimum becomes the lowest. For Al content larger than 52 %, the lowest donor level is associated with X minimum.

4.2.3. Potential Well

It is necessary to study the electric field enhanced emission rate in order to determine the type of potential well for the DX center, as discussed in section 4.1.4. Among the various potential wells, a special attention will be paid to the Coulombic potential well and the Yukawa potential well since both kinds of potential well are predominantly responsible for the electric-field enhanced emission rate in the electric field range of interest (10^4-10^6 V/cm) [51].

The Yukawa potential [41] is a modified Coulombic potential which includes the effect of screening of charges by surrounding electrons. In the presence of an electric field, the potential is given by

$$V(r) = -q^2\exp(-r/R_o)/(4\pi\ \varepsilon_r\varepsilon_o) - qFr\cos\theta \qquad (4.33)$$

where R_o is the shielding length, which will be treated as an adjustable parameter. To describe the Poole-Frenkel lowering and the phonon assisted tunnelling, one must find the point of maximum

potential by solving the following equation numerically.

$$q \exp(-r/R_o) \ [1/r^2 + 1/(rR_o)]/(4\pi \varepsilon_r \varepsilon_o) = F\cos\theta \qquad (4.34)$$

As expected, the total electric-field enhanced emission rate obtained by adjusting the screening length shows that the effect of phonon assisted tunnelling is more predominant than that of the Poole-Frenkel lowering effect at high electric field, as is shown in Fig.4.5. This means that the deeper the defect level is, the more important the tunnelling effect is. As for the DX center, nevertheless, which has a smaller value of activation energy than that of the EL2 center, both the Poole-Frenkel and phonon-assisted tunneling effects must be considered simultaneously.

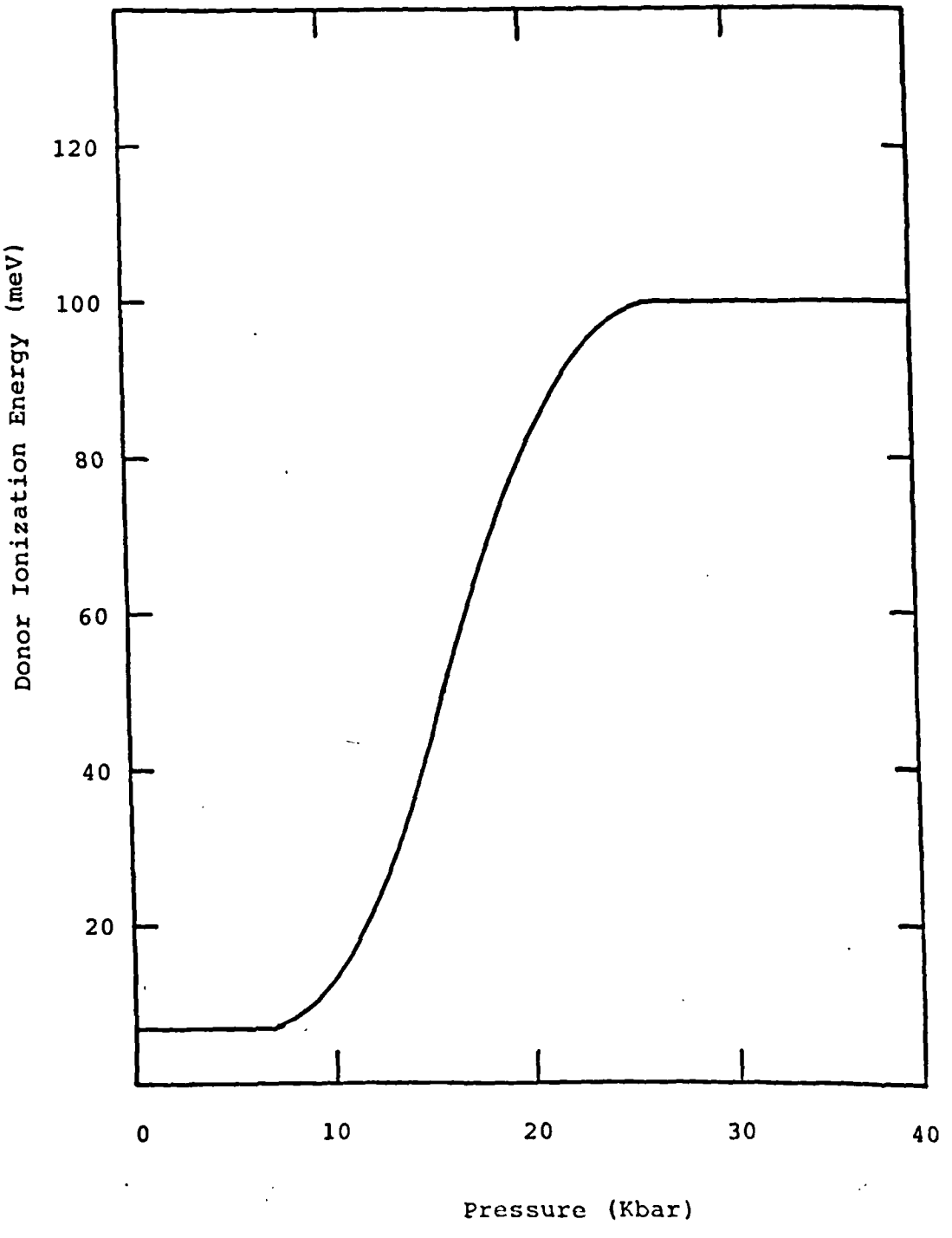

Figure 4.3 The pressure dependence of the Sn donor ionization energy in $Al_{0.3}Ga_{0.7}As$.

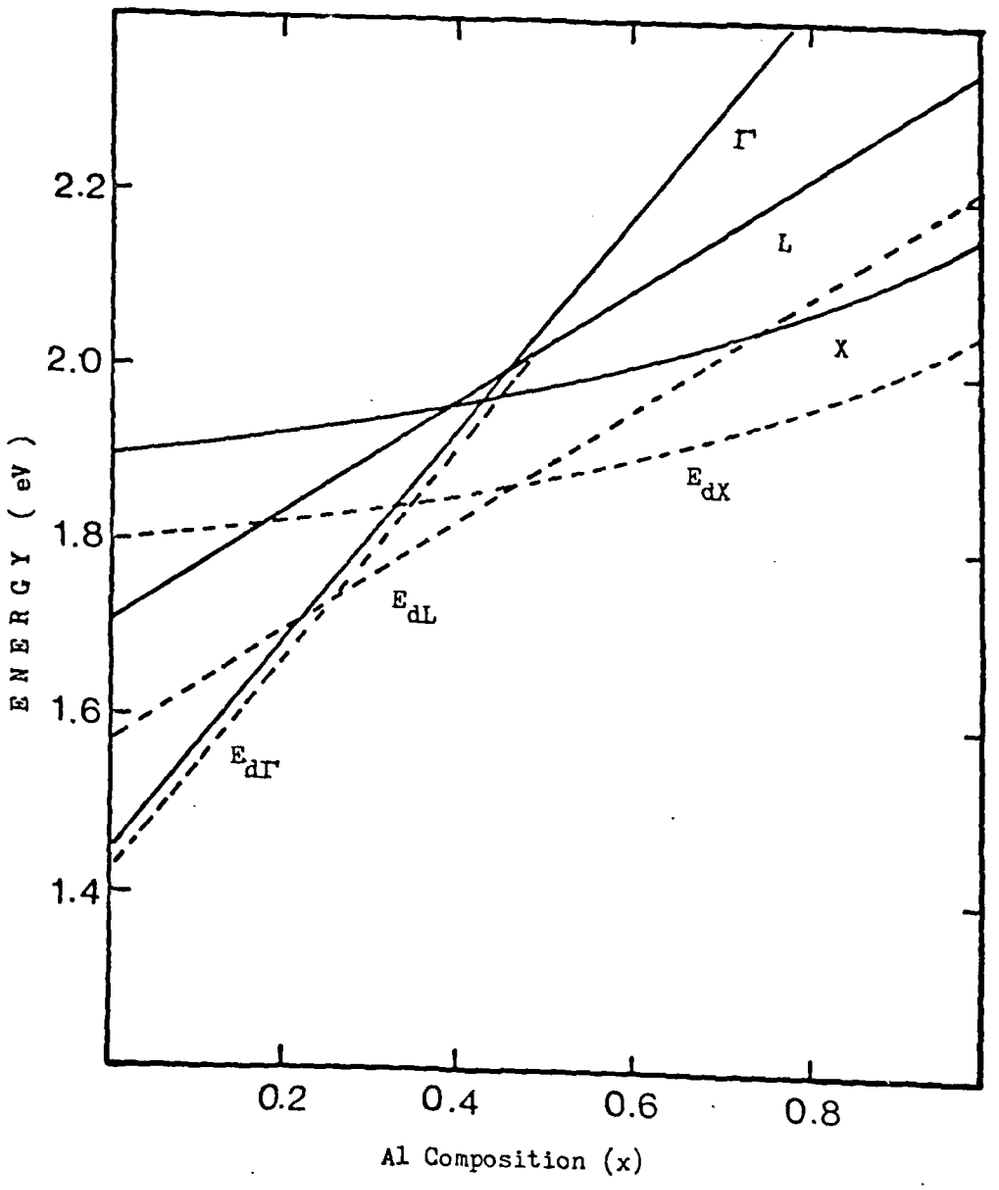

Figure 4.4 Compositional dependence of the direct Γ , and indirect L and X conduction band minima in AlGaAs at 300 K.

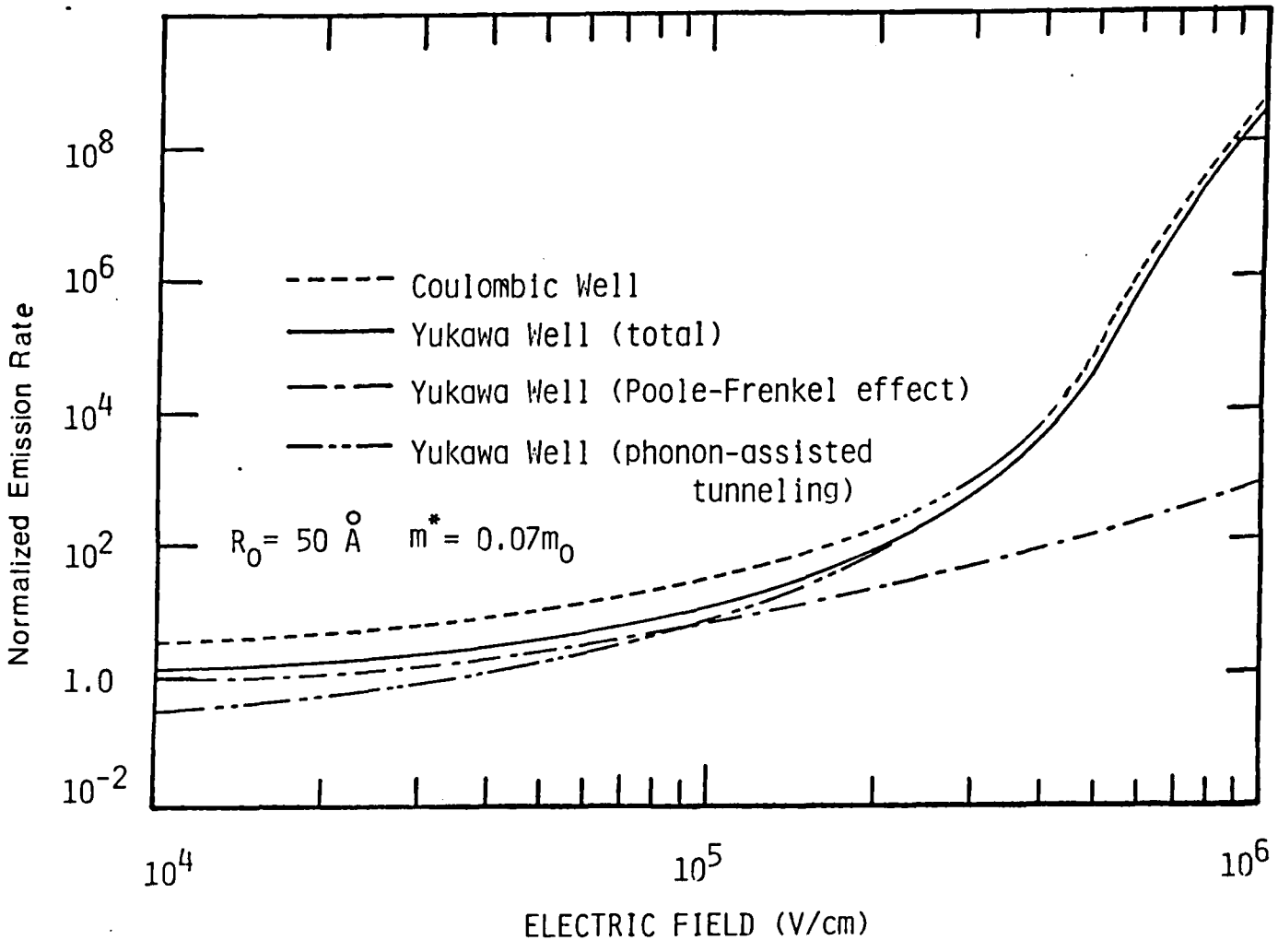

Fig.4.5 Electric field enhanced emission rates for the Yukawa potential well and Coulombic potential well.

CHAPTER V
RESULTS AND DISCUSSION

The physical origins for the EL2 center, which is one of the most important electron traps in GaAs, will be discussed in section 5.1. The type of potential well and charge state for the EL2 center will also be determined by comparing the calculated DLTS spectrum with the experimental data. In section 5.2, to understand the nature of electron emission (capture) from the DX center in $Al_xGa_{1-x}As$, the final transition state of conduction band will be discussed. In addition, a prediction on the type of potential well and charge state will be made based on the experimental results of low temperature capacitance-voltage and DLTS measurements.

5.1. Physical Origins of EL2 Center

It has been shown in the previous chapter that the EL2 center may be ascribed to two different types of native point defects. One is designated as the EL2b (E_c-0.76eV) electron trap, and the other is denoted as the EL2a (E_c-0.83eV) electron trap. The physical origin for the EL2a trap is attributed to the arsenic antisite (As_{Ga}) defect or arsenic antisite plus neighboring four arsenic (As_{Ga}-As_4) cluster, whereas, the physical origin for the EL2b level may be attributed to the arsenic antisite plus arsenic vacancy (As_{Ga}-V_{As}) complex. Based on this model, the dependence of the density of EL2a and EL2b

electron traps on the $[AsH_3]/[TMGa]$ (≈ r) mole fraction ratio in the MOCVD and VPE grown GaAs is established. The result shows that density of EL2a trap is directly proportional to the mole fraction ratio of $r^{1/2}$, whereas, the density of EL2b trap varies with the mole fraction ratio of $r^{1/4}$. This prediction is supported by the experimental data for the MOCVD and VPE grown GaAs (see Chapter VI).

Figure 5.1 shows the theoretical calculations of the DLTS spectra for the EL2a electron trap, for the case of Coulombic well, Dirac well, square well and the polarization well, respectively, as well as the zero electric field case. A comparison of the measured DLTS spectrum with the calculated nonexponential DLTS spectrum by taking into account the electric field dependent emission rates reveals that the best fitted potential well for the EL2a trap is the Coulombic well with a double-charged state, as is shown in Fig.5.2. Therefore, the most likely physical origin for the EL2a trap is ascribed to the double-charged As_{Ga}^{++} antisite [40] or its cluster with As_4. Value of the capture cross section (σ_n) for the EL2a trap was assumed equal to 8×10^{-14} cm^2 [4]. This value is comparable to our measured capture cross section of EL2a level for the MOCVD grown GaAs (10^{-13} cm^2).

5.2. DX Center and L Conduction Band Minimum

Low temperature C^{-2} - V data for the Sn-doped $Al_{0.3}Ga_{0.7}As$ are shown in Fig.5.3. A sufficiently large reverse bias was first applied at room temperature when the DX center is fully ionized for $0<x<d$. The reverse bias was then decreased to a forward bias at a low

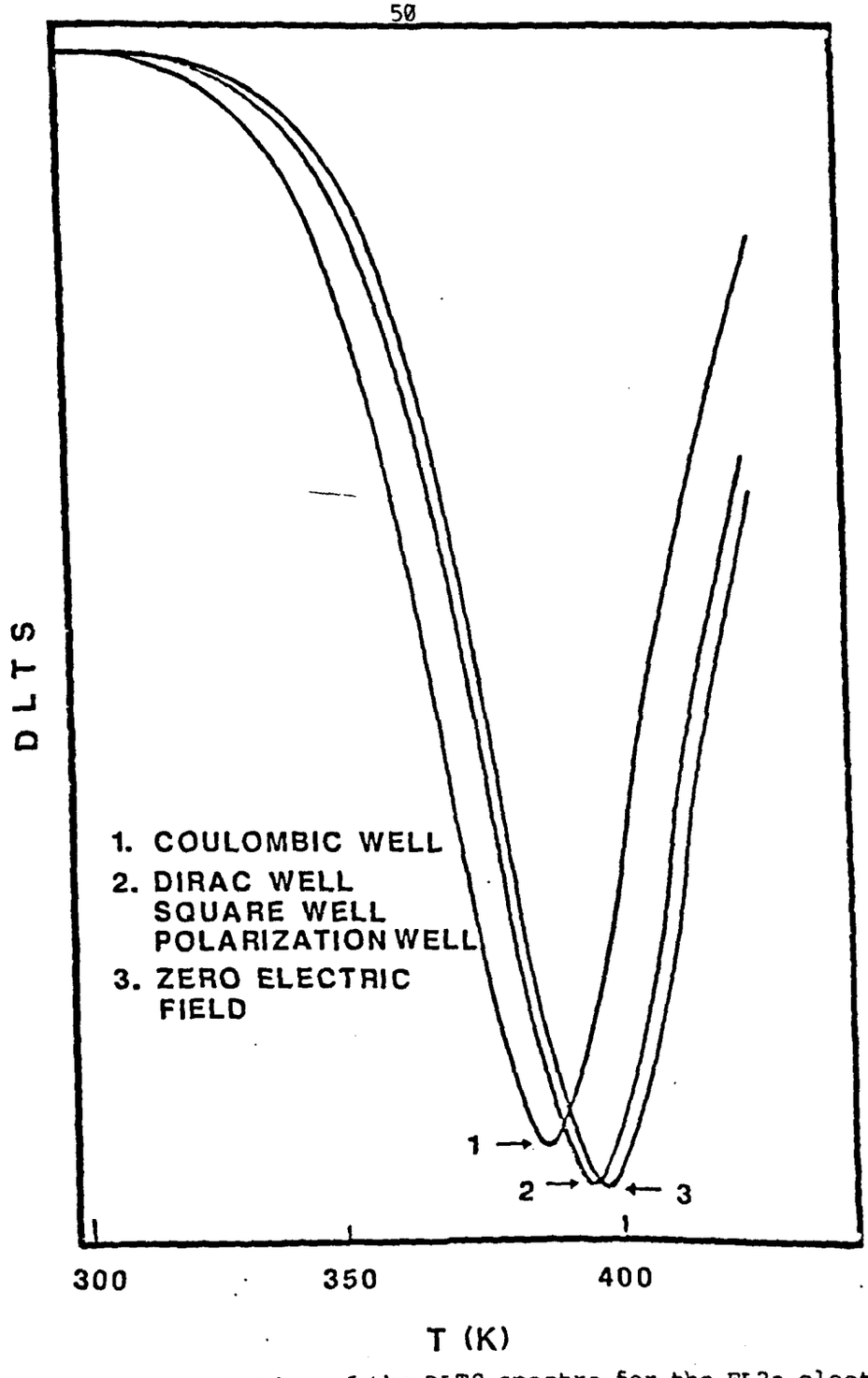

Figure 5.1 Simulation of the DLTS spectra for the EL2a electron trap, assuming Coulombic well(1), Dirac, square, and polarization well(2), and for zero electric field case(3).

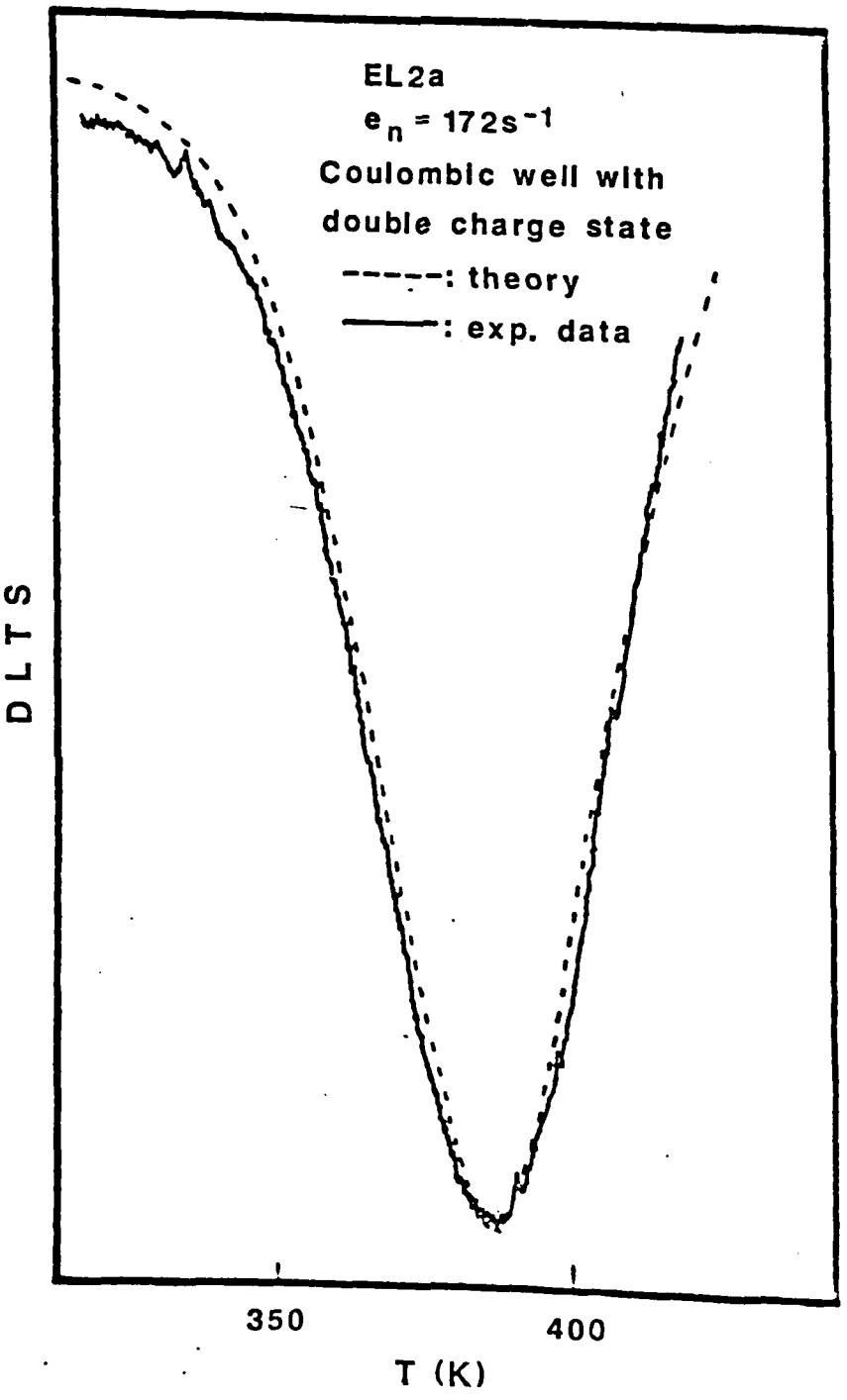

Figure 5.2 Comparison of the calculated DLTS spectrum (assuming Coulombic well with double-charged state) and the measured DLTS spectrum for the EL2a electron trap in GaAs.

temperature such that the DX center was filled with electrons. After that, the reverse bias was increased again. At around 77 K, the DX center remains filled with electrons everywhere in the depletion region. The excess voltage, V_e is shown in the figure. The Fermi level E_f in the charge neutral region can be determined by

$$E_c - E_f = kT \ln(N_c/N_d) \qquad (5.1)$$

where N_c is the effective density of conduction states in the Γ conduction band.

The value of energy barrier, ΔE_b for electron emission can be determined from the slope of capture rate versus inverse temperature (see Eqn.(4.26)). It was found, however, that it was rather difficult to determinie accurately the energy barrier for our samples due to the presence of another defect level which is located very closely. The adjacent deep-level, whose density is much smaller than that of the DX center, might have affected the transient signal of the DX center significantly. Hence, the activation energy, E_{t1} was determined using the published data of 0.02 eV for ΔE_b [42].

By comparing the experimental results of activation energies, E_{t2} obtained from the low temperature capacitance-voltage measurement and E_{t1} obtained from the DLTS spectra for the DX center, it is found that there is a difference between these two activation energies. This difference in activation energy can be explained if it is assumed that the emission of electrons from the DX center is related to the higher band than the Γ minimum in the conduction band. From the conduction band diagram as a function of Al composition (Fig.4.4), one can

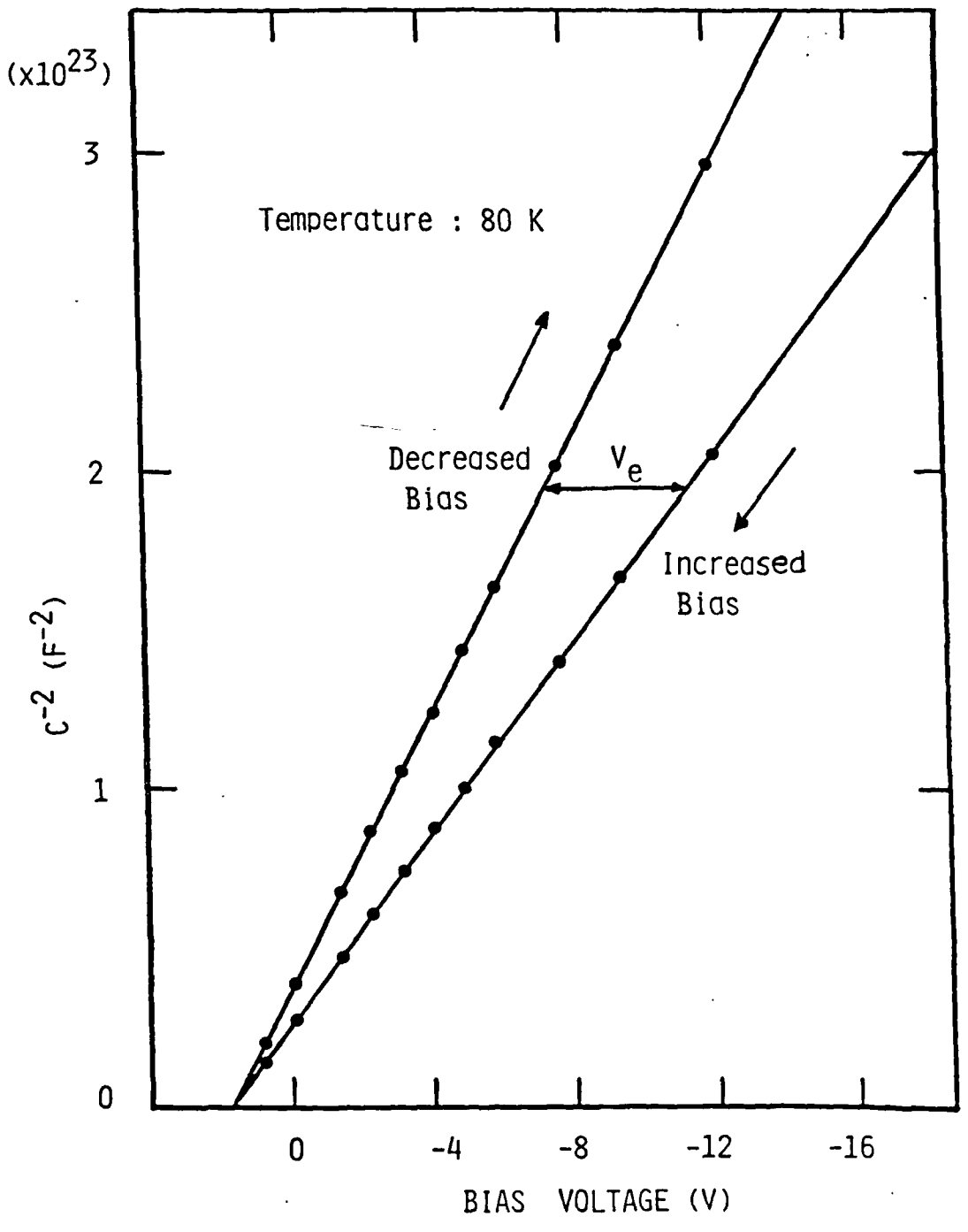

Figure 5.3 Low temperature capacitance-voltage characteristics

easily see that the energy separation of Γ-L minima is only slightly larger than the value of E_{t1}- E_{t2}, as is shown in table 5.1. Hence, it is believed that the final electron transition state from the DX center is due to the L minimum, within the allowable experimental error.

Figure 5.4 shows the measured DLTS spectrum for the Sn-doped $Al_{0.3}Ga_{0.7}As$ and the calculated DLTS spectra by assuming that (1) the type of potential well for the DX center is the single-charged Coulombic or Yukawa potential, and (2) the electron emission from the DX center is related to the L conduction minimum. It was found that the calculated DLTS spectra can be fitted nicely to the measured data, provided that the screening length R_o for the Yukawa potential is less than 100 A^o. It is, therefore, concluded that the DX center emits electrons to the L conduction minimum instead of the Γ minimum, and it has a single and positive charge state.

The activation energy of the DX center has been found to be dependent not on the amounts of incorporated aluminum atoms but on the kinds of doping impurities and growth techniques. Moreover, its concentration and capture cross section have shown strong dependence on the growth condition, e.g., ratio of arsine to trimethylgallium and growth temperature. It is worthwhile to note that there is a certain trend in which the activation energy of the DX centers with group IV impurities decreases as the mass of the group IV impurity increases, while the activation energy of the DX center for group VI impurities are remains constant with value of 0.28 eV as has been shown in table.2.2.

Based on the experimental and theoretical results so far we obtained, however, it is still difficult to determine whether the origin of the DX center is the donor-anion vacancy complex or subtitutional donor impurity itself. This ambigutiy might stem from the fact that the formation of grow-in defect is nonstoichiometric [28].

Table.5.1. Paramters for the DX center in Sn-doped $Al_{0.3}Ga_{0.7}As$ determined by C-V and DLTS measurements.

Parameters		Results (eV)
DLTS Measurement	$E_{t1} + \Delta E_b$	0.21
	ΔE_b	0.02
	E_{t1}	0.19
C - V Measureme	qV_L	0.075
	E_f	0.013
	E_{t2}	0.088
$E_{t1} - E_{t2}$		0.102
E_{Lr}		0.1025

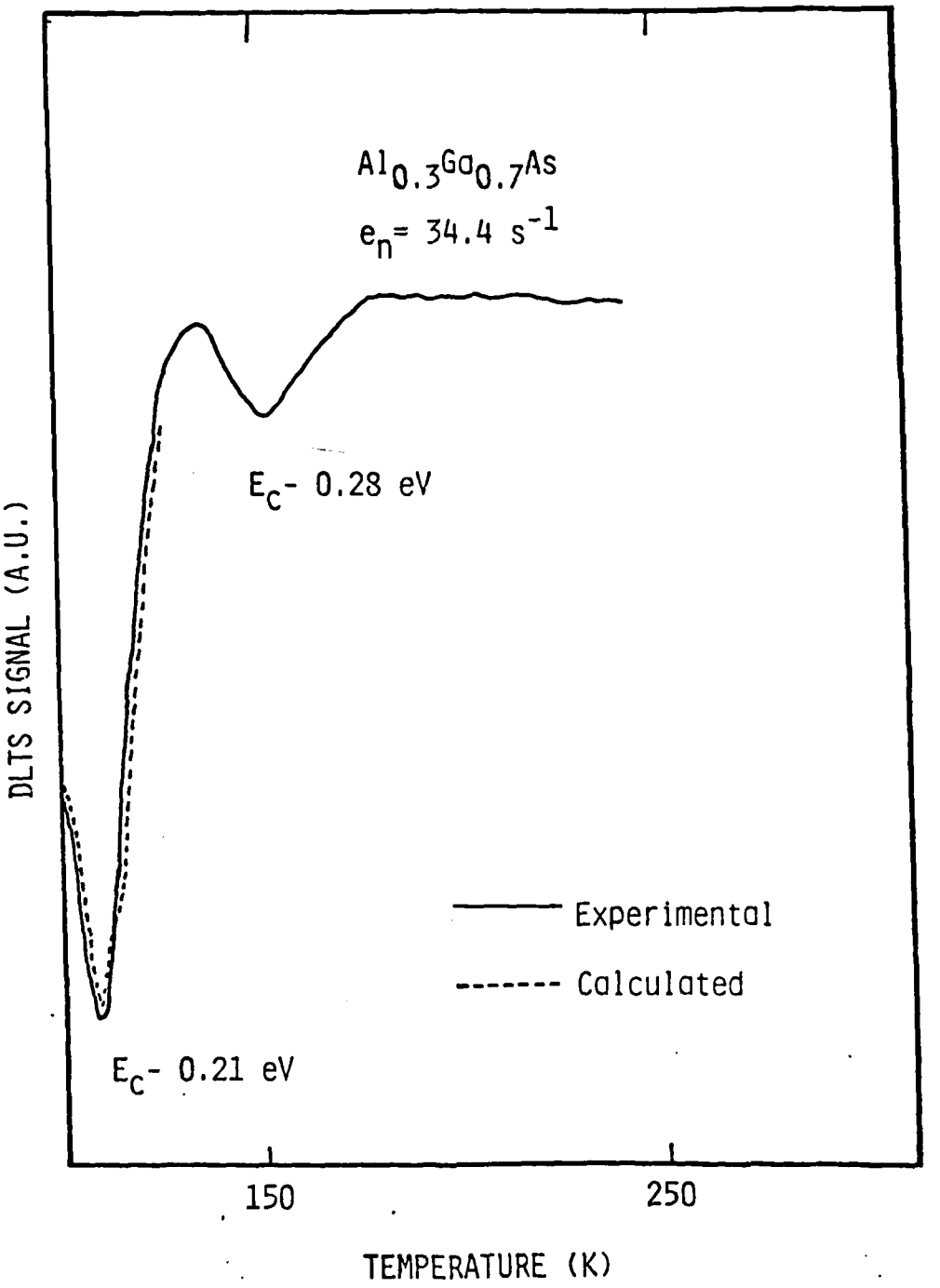

Figure 5.4 Comparison of the calculated DLTS spectrum (assuming Coulombic or Yukawa potential with single-charged state and electron emission to the L minimum) and the measured DLTS spectrum for the EL2a electron trap in AlGaAs.

CHAPTER VI
GROWN-IN DEFECTS IN MULTI-EPILAYER GaAs GROWN BY MOCVD UNDER DIFFERENT GROWTH CONDITIONS

Studies of the grown-in defects in multi-epilayer GaAs (with/without a buffer layer) grown by Metalorganic Chemical Vapor Deposition under different [AsH_3]/[TMGa] ratios, growth temperatures, and growth rates have been made in this chapter by the Deep Level Transient Spectroscopy method. For samples without a buffer layer, two electron traps with activation energies of E_c- 0.83 eV (EL2a) and E_c- 0.74 eV are observed, whereas, for samples with a 6 μm thick buffer layer, only EL2a level is found. The concentration of the deep-level traps is found closely related to the [AsH_3]/[TMGa] ratio, the growth temperature and the growth rate (mainly at lower growth rate). The results show that, for samples without a buffer layer, the background dopant density profile is closely related to the deep-level trap density profile in the epilayers, whereas for samples with a buffer layer, the profile of background dopant density is less influenced by the presence of the deep-level trap.

6.1. Introduction

Metalorganic Chemical Vapor Deposition (MOCVD) has become an important technique for the growth of GaAs epitaxial layer because of its ability for large scale production, precise thickness controllability and excellent uniformity in the grown layer [45].

However, grown-in deep-level defects observed in the MOCVD GaAs are different among samples grown under various growth conditions. It is, therefore, important to investigate the grown-in defects versus growth parameters in MOCVD GaAs so that optimum growth condition can be achieved. This is essential for improving the performance of optoelectronic, microwave as well as very high speed devices fabricated from GaAs material.

The goal of this study is to correlate the depth profile of the dominant deep-level defects to various growth parameters in the unintentionally doped multi-epilayer GaAs grown by MOCVD. Mole fraction ratio of arsine and trimethylgallium, $[AsH_3]/[TMGa]$, growth temperature and growth rate are the three growth parameters used this study. In addition, the effect of buffer layer and the out-diffusion of impurities from the semi-insulating (S.I.) substrate on the epilayer property is also investigated.

6.2. Experimental Details

The samples used in this study were summarized in Chapter III under various growth conditions. Deep level transient spectroscopy (DLTS) technique was used to determine the deep-level defects in the GaAs epilayers using Au-GaAs Schottky barrier structure. Profiles of the deep-level defect density were determined by using different reverse-biased pulses (up to -20 V) and the expression [31]

$$N_T(X_c) = \frac{q\, W^2\, N_D(W)\, N_D(X_c)}{\varepsilon_o\, \varepsilon_s} \; \frac{\delta\,(\Delta C/C)}{\delta V_c} \qquad (6.1)$$

where $W = [2\epsilon_s(V_{bi} - V_R - kT/q)/qN_D]^{1/2}$ is the depletion layer width at the quiescent reverse bias. X_c is the value of X at the depletion edge of the n- region during the clear pulse. $N_D(W)$ is the density of donor impurities at W. $N_D(X_c)$ is the density of donor impurities at X_c, and V_c is the magnitude of the clear pulse. δV_c is the change in V_c to cause a change in X_c (a typical value of 0.05 μm). To obtain a fine resolution of the deep-level profile, the reverse bias voltage steps were divided into many small incremental voltages, and the edge effect was considered.

6.3. Results and Discussion

Figure 6.1 shows the DLTS spectrum for the electron traps observed in sample OM-2-296. The E_c-0.83 eV level with emission cross section of 2.1×10^{-13} cm^2, known as the EL2a electron trap was observed in all the samples studied, whereas one additional electron trap, E_c-0.74 eV level with emission cross section of 3.1×10^{-13} cm^2, was detected only in samples without a buffer layer (see Fig.6.2). It is found, by Scanning Electron Microscopy analysis, that the initially undoped S.I. substrate was contaminated by Cr-impurities during the process. Cr-level in n-type GaAs is known to have an activation energy of 0.72 - 0.88 eV below the conduction bandedge [46,47]. It is, however, difficult to assign the 0.74 eV level to Cr-impurity itself due to a large emission cross section. Hence, the E_c-0.74 eV level observed in our samples is believed to be due to the complex defect possibly formed by the gallium vacancy with Cr-impurity out-diffused from the S.I. GaAs substrate into the epilayers [48].

For sample with a buffer layer (Fig.6.2.a), it is noted that the density profiles for both the background dopant and the EL2a level are very similar in shape, except a small shift and a deviation near the surface of the epilayer. This is consistent with the results of Watanabe et al.[11] and Bhattacharya et al.[4]. They reported that the density of the EL2 level was dependent on the $[AsH_3]/[TMGa]$ ratio with a certain proportionality factor depending on the growth temperature. In our samples grown at 675 ^{o}C, it was found that the density of the EL2a level is proportional to the $\{[AsH_3]/[TMGa]\}^{1/2}$. This result is in good agreement with the prediction made in the last chapter. For samples without a buffer layer (Fig.6.2.b and Fig.6.3), there is a considerable difference between the intended doping profile and the actual doping profile due to the compensation by the deep-level impurities out-diffused from the S.I. GaAs substrate into the epilayer [49]. Furthermore, it was observed that the density profiles for the EL2a trap do not follow the predicted trend of the $[AsH_3]/[TMGa]$ ratio, but conform to the actual compensated doping profiles.

For sample OM-2-312 (Fig.6.4), in which the growth temperature was the only parameter varied, the increase in growth temperature raises the arsenic pressure during the deposition of epilayers, which in turn results in a more arsenic-rich condition. Therefore, in this case, the density profiles of the background dopant and the EL2a level are proportional to the growth temperature [50].

In sample OM-2-295, even though there is no buffer layer, no significant compensation effect was observed, and only one electron

trap, namely, the EL2a level was found with a rather irregular density profile. This may be due to the fact that compensation mechanism and the out-diffusion of impurities from the S.I. substrate can not keep up with the rapid growth of epilayers in this sample.

It is important to note that a buffer layer inhibits the impurity out-diffusion from the S.I. substrate into the epilayers, and consequently excludes the formation of defects related to the substrate impurities. Furthermore, the intended doping density profile for the epilayer can be obtained by growing a buffer layer on the S.I. substrate, since this diminishes the compensation effect.

6.4. Conclusions

The dominant electron traps observed in our MOCVD grown multiepilayer GaAs are due to the E_c-0.83 eV (EL2a) and the E_c-0.74 eV level for samples without a buffer layer. For samples with a buffer layer, only EL2a electron trap was observed. The formation and the distribution of deep-level defects have been found to be strongly influenced by the growth conditions. The density profile of the EL2a level in samples with a buffer layer was found to be proportional to $\{[AsH_3]/[TMGa]\}^{1/2}$ and the growth temperature. Although the effect of growth rate on the deep-level traps can not be observed clearly in sample grown at a higher growth rate, the out-diffusion of impurities and the compensation due to the S.I. substrate, however, have been reduced considerably. In addition, it is found that adding a buffer layer on the S.I. GaAs substrate is effective in preventing

the out-diffusion of the deep-level impurities from the substrate into the epilayers grown by MOCVD technique.

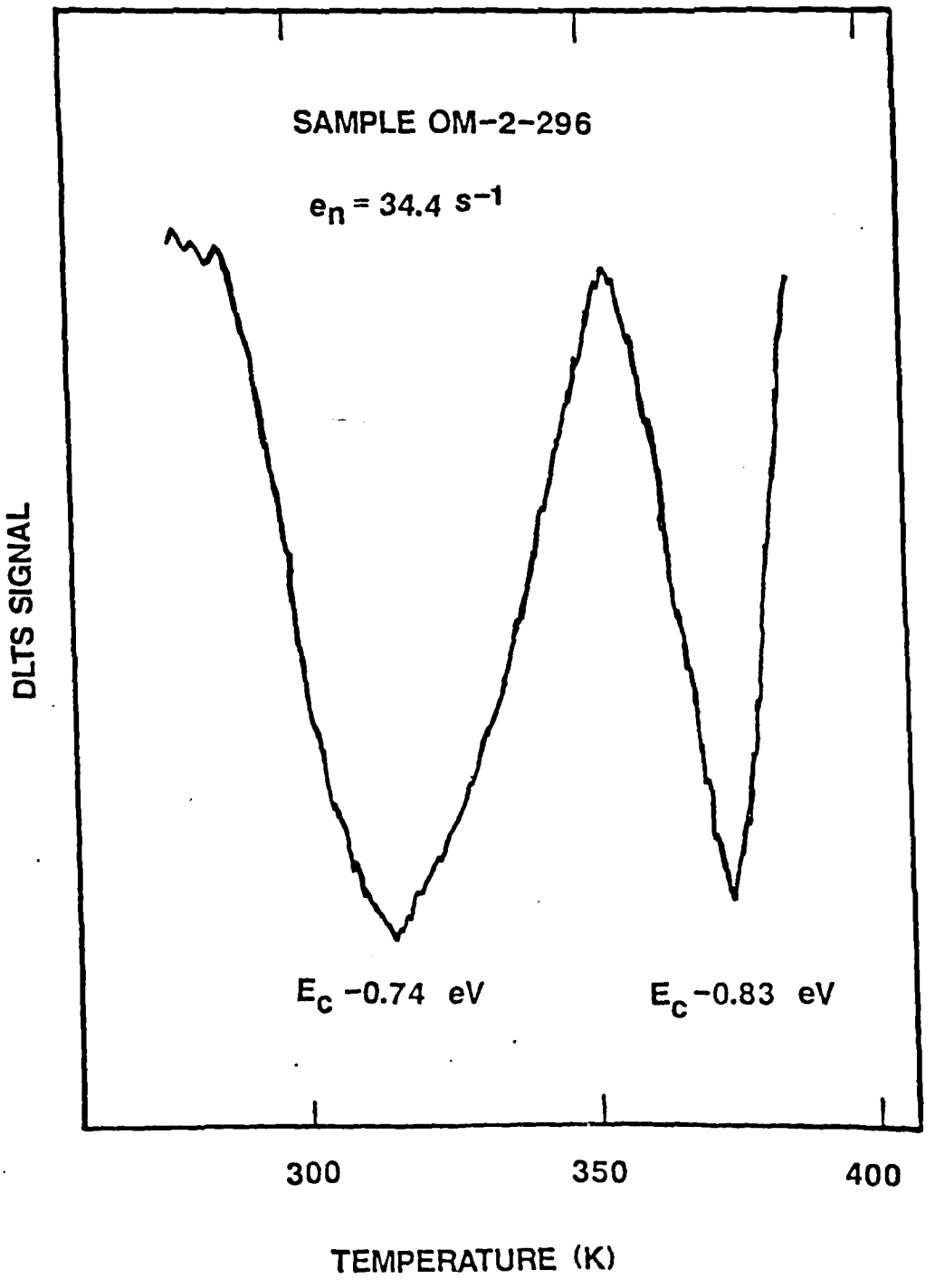

Figure 6.1 DLTS spectrum of the electron traps in GaAs sample OM-2-296 (No buffer layer). Two elctron traps are found; one is the E_c-0.74 eV level, and the other is E_c-0.83 eV level (EL2a trap).

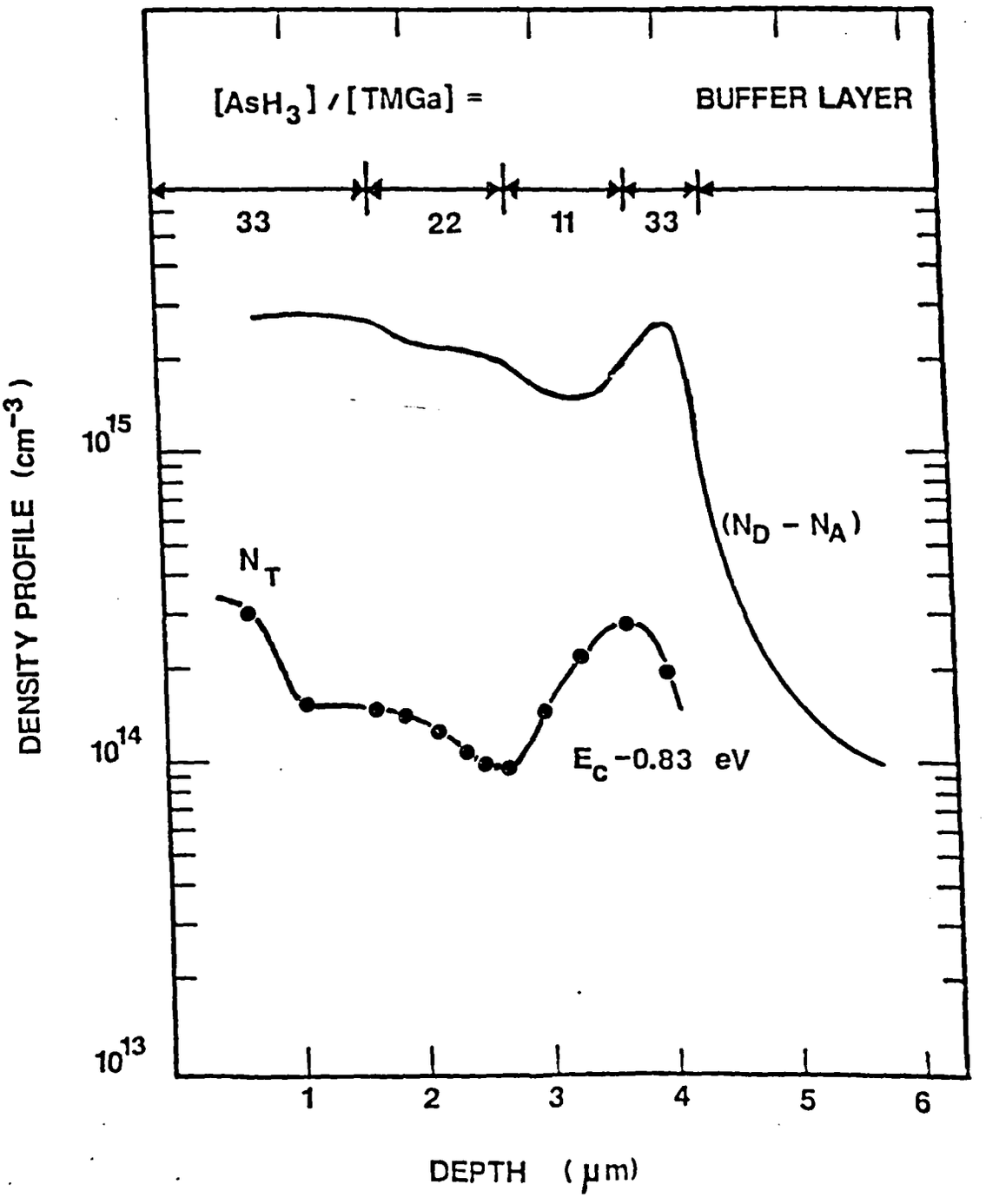

Figure 6.2.a Density profiles for the background dopant, the E_C-0.83 eV level and the E_C-0.74 eV level for sample OM-2-310 (with a buffer layer)

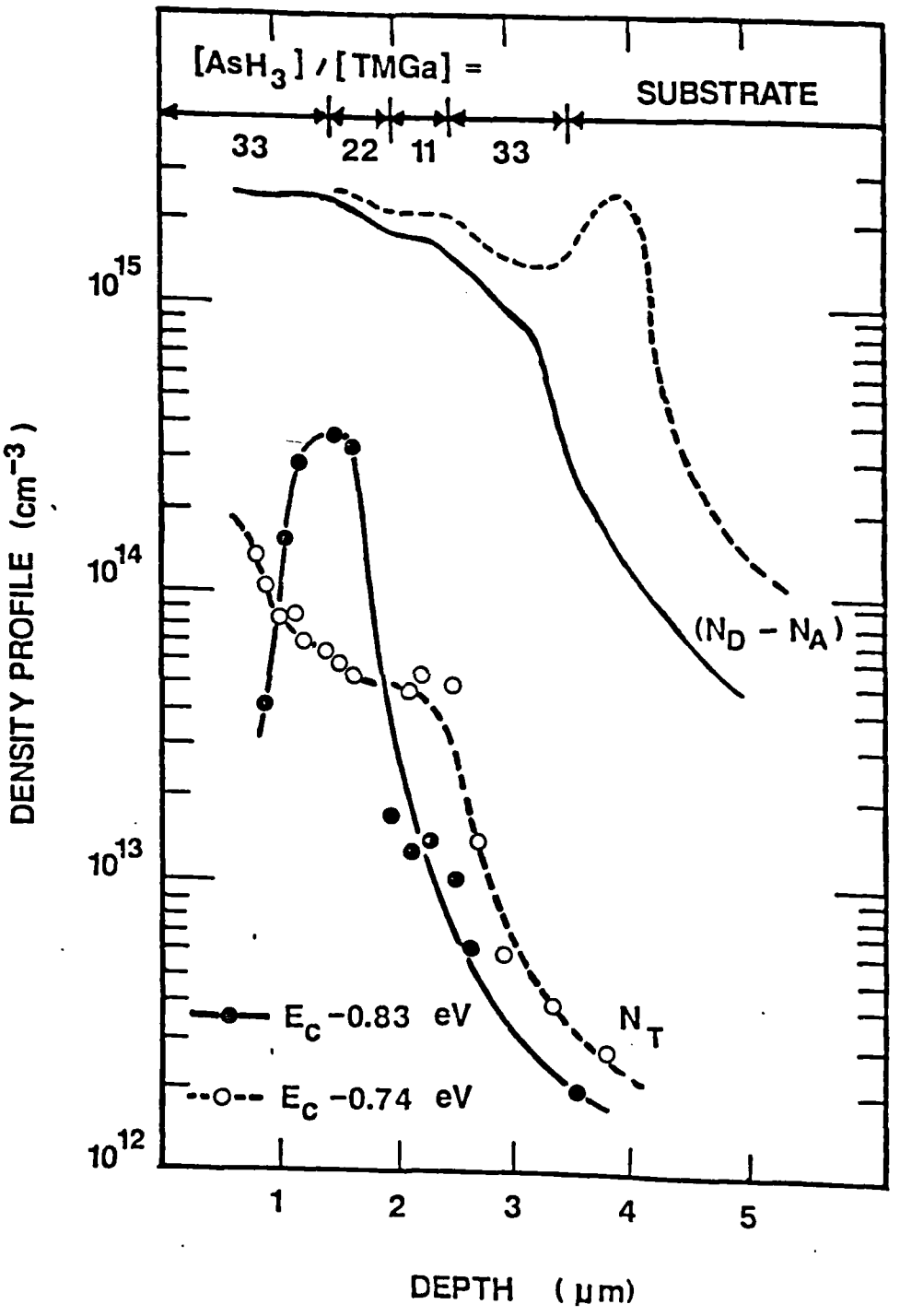

Figure 6.2.b Sample OM-2-309 (without a buffer layer). Except for a buffer layer, both samples are grown under identical growth conditions. Dash- and solid-lines denote the intended and the actual dopant profiles, respectively.

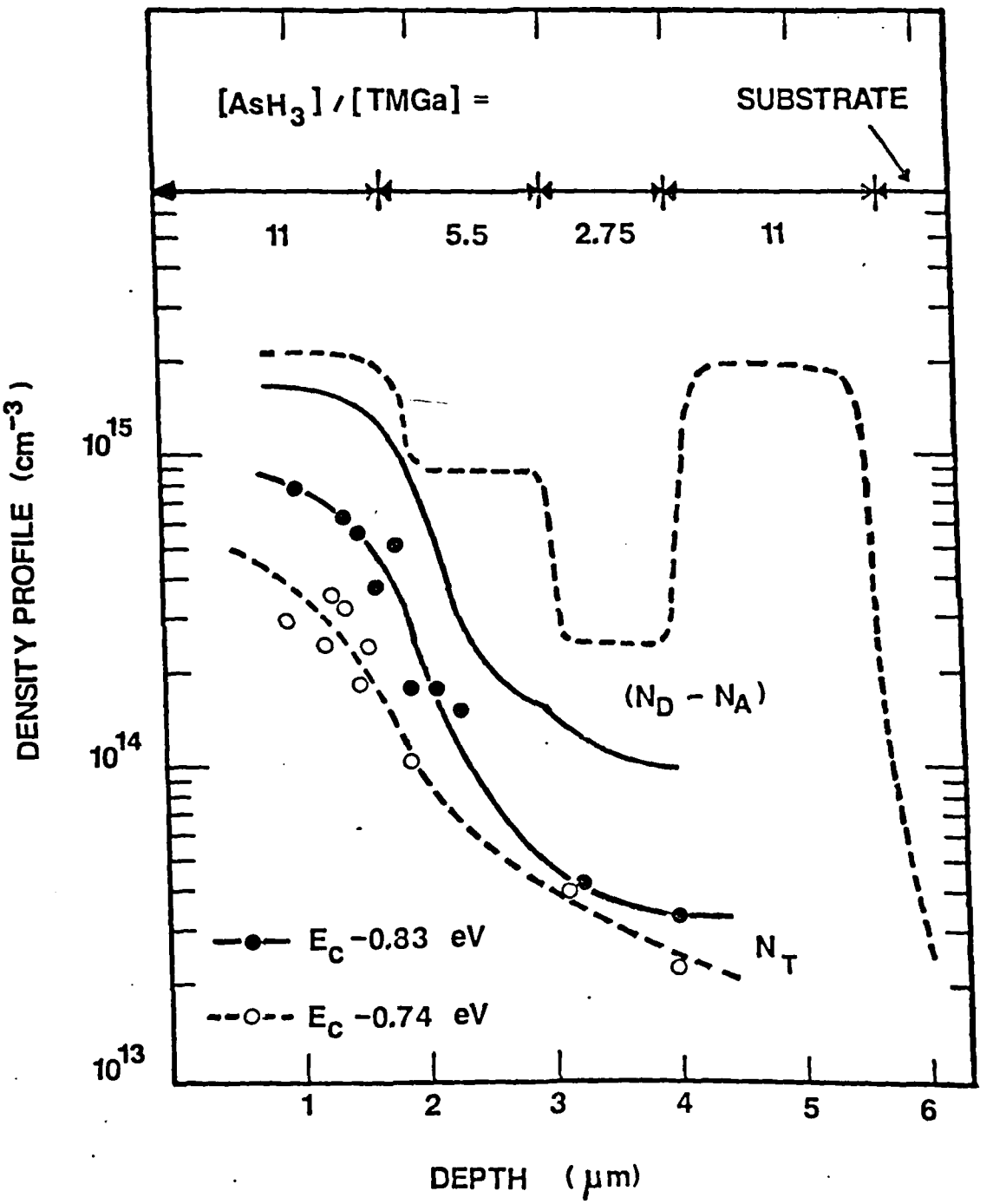

Figure 6.3 Density profiles for the background dopant, the E_c-0.83 eV and the E_c-0.74 eV level for sample OM-2-296. Dash- and solid-lines denote the intended and the actual dopant profiles, respectively.

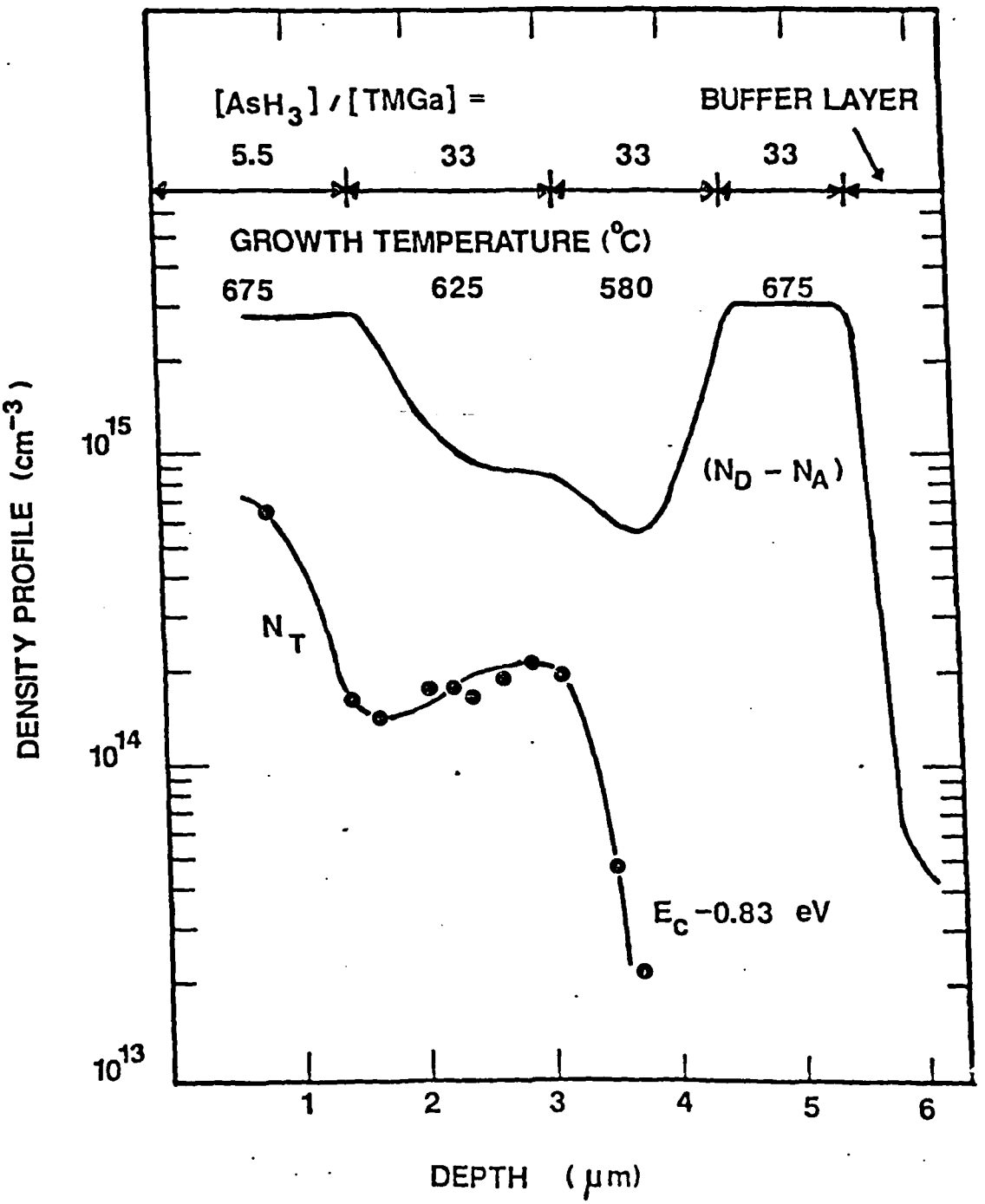

Figure 6.4 Density profiles for the background dopant and the E_c-0.83 eV level for sample OM-2-312.

CHAPTER VII
SUMMARY AND CONCLUSION

A detailed theoretical and experimental study on the grown-in deep-level defects has been carried in this report, with special emphasis being placed on the EL2 center in GaAs and the DX center in $Al_xGa_{1-x}As$.

A defect model is presented to describe the physical origins of the EL2 electron trap in GaAs The EL2 level is ascribed to two types of native point defects. One is designated as the EL2b (E_c-0.76eV) electron trap, and the other is denoted as the EL2a (E_c-0.83eV) electron trap. The physical origin for the EL2a trap is attributed to the arsenic antisite (As_{Ga}) defect or arsenic antisite plus neighboring four arsenic (As_{Ga}-As_4) cluster, whereas, the physical origin for the EL2b level may be attributed to the arsenic antisite plus arsenic vacancy (As_{Ga}-V_{As}) complex. Based on this model, the dependence of the density of EL2a and EL2b electron traps on the [As]/[Ga] (= r) mole fraction ratio in the MOCVD and VPE grown GaAs was established. The result shows that density of EL2a trap is directly proportional to the mole fraction ratio of $r^{1/2}$, whereas, the density of EL2b trap varies with the mole fraction ratio of $r^{1/4}$. This prediction is supported by the experimental data for the MOCVD and VPE grown GaAs. From the analysis of the electric field enhanced emission rates and the DLTS data for the EL2a electron trap in GaAs,

it is further shown that the type of potential well for this trap can be best described by a Coulombic potential well with a double-charged state such as As_{Ga}^{++} antisite defect.

A correlation of density profile to various growth parameters has been performed for the dominant grown-in deep level defects in multi-epilayer GaAs grown by MOCVD under different growth conditions. The formation and the distribution of deep-level defects have been found to be strongly dependent on the growth conditions; the density profile of the EL2a level was proportional to $\{[AsH_3]/[TMGa]\}^{1/2}$ and the growth temperature, as has been predicted in Chapter V. It has been also found that a buffer layer reduces the effect of compensation which results from the out-diffusion of substrate impurities into the epilayer. On the DX center in $Al_xGa_{1-x}As$, the electron emission and capture transitions associated with three conduction band minima have been investigated, along with the identification of its most probable type of potential well and charge state. It has been found that the emission and capture of electrons for the DX center is linked to the L minimum in the conduction band instead of the lowest-lying Γ minimum. The Coulombic or Yukawa potential well with single charge state is found to be the best candidate for the DX center.

References

1. A. Humbert, L. Hollan, and D. Bois, "Influence of the Growth Conditions on the Incorporation of Deep-Levels in VPE GaAs", J. Appl. Phys., Vol.47, pp.4137, 1976.

2. M. D. Miller, G. H. Olsen, and M. Ettenberg, " The Effect of Gas-Phase Stoichiometry on Deep Levels in Vapor-Grown GaAs", Appl.Phys. Lett., Vol.31, pp.538, 1977.

3. D. V. Lang and R. A. Logan, "A Study of Deep Levels in GaAs by Capacitance Spectroscopy", J. Electron. Mater., Vol.4, pp.1053, 1975.

4. P. K. Bhattacharya, J. W. Ku, J. T. Owen, V. Aebi, C. B. Cooper III, and R. L. Moon, "The Trend of Deep States in Organometallic Vapor-Phase Epitaxial GaAs with Varying As/Ga Ratios", Appl. Phys. Lett., Vol.36, pp.304, 1980.

5. H. Z. Zhu, Y. Adachi, and T. Ikoma, "Deep Levels in MOCVD GaAs Grown under Different Ga/As Mole Fractions", J. Crystal Growth, Vol.55, pp.154, 1981.

6. A. Zylbersztejn, R. H. Wallis, and J. M. Besson, "Trap Depth and Electron Capture Cross Section Determination by Trap Refilling Experiments in Schottky Diodes", Appl. Phys. Lett., Vol.33, pp.200, 1978.

7. S. S. Li, W. L. Wang, P. Lai, R. Y. Loo, G. S. Kamath, and R. C. Knechtli, "Deep-Level Defects, Recombination Mechanisms, and Their Correlation to the Performance of Low-Energy Proton-Irradiated AlGaAs-GaAs Solar Cells", IEEE Trans. Electron Devices, Vol.27, pp.857, 1980.

8. D. V. Lang, "Review of Radiation-Induced Defects in III-V Compounds", Inst. Phys. Conf. Ser., Vol.31, pp.70, 1977.

9. J. Lagowski, H. C. Gatos, J. M. Parsey, K. Wada, M. Kaminska, and W. Walukiewicz, " Origins of the 0.82 eV Electron Trap in GaAs and its Annihilation by Shallow Donors", Appl. Phys. Lett., Vol.40, pp.342, 1982.

10. E. R. Weber, and J. Schneider, "As_{Ga} Antisite Defects in GaAs", Physica, Vol.116B, pp.398, 1983.

11. M. O. Watanabe, A. Tanaka, T. Udagawa, T. Nakanisi, and Y. Zohta, "AsH_3 to $Ga(CH_3)$ Mole Ratio Dependence of Dominant Deep Levels in MOCVD GaAs", Jpn. J. Appl. Phys., Vol.22, pp.923, 1982.

12. B. K. Meyer, D. M. Hofmann, F. Lohse, and J.-M. Spaeth, "Optical, ODESR and ODENDOR Investigation of As_{Ga} Antisite Defects and the EL2 Defect in GaAs", 13th International Conference on Defect in Semiconductor, Vol.14a, pp.921, 1985.

13. J. Lagowski, D. G. Lin, T. Aoyama, and H. C. Gatos, "Identification of Oxygen-Related Midgap Level in GaAs", Appl. Phys. Lett., Vol.44, pp.336, 1984.

14. M. Taniguchi, and T. Ikoma, "Spectral Distributions of Photoquenching Rate and Multimetastable States for Midgap Electron Traps(EL2 Family) in GaAs". Appl. Phys. Lett., Vol.45, pp.69, 1984.

15. J. Lagowski, and H. C. Gatos, "Nonstoichiometric Defects in GaAs and the EL2 Bandwagon", 13th international Conference on Defects in Semiconductors, Vol.14a, pp.73, 1985.

16. D.V.Lang and R.A,Logan, "Trapping Characteristics and a Donor Complex(DX) Model for the Persistent-Photoconductivity Trapping Center in Te-Doped AlGaAs", Phys. Rev. Lett., Vol.39, pp.635, 1977.

17. A.Kumagai, H.Kawai, Y.Mori, and K.Kaneko, "Chemical Trends in the Activation Energies of DX Center", Appl. Phys. Lett., Vol.45, pp.1322, 1984.

18. M.Mizuta, M.Tachigawa, H.Kukimoto, and S.Minomura, "Direct Evidence for the DX Center Being a Substitutional Donor in AlGaAs Alloy System", Jpn. J. Appl. Phys., Vol.24, L143, 1985.

19. A. Mircea, and D.Bios, " A Review of Deep-Level Defects in III-V Semiconductors", Inst.Phys. Conf. Ser., Vol.46, pp.82, 1979.

20. D. Pons, "Anisotropic Defect Introduction in n and p-GaAs by Electron Irradiation", Physica, Vol.116B, pp.388, 1983.

21. S.Naritsuka, K.Yamanaka, M.Mihara, and M.Ishii, "Effects of Growth Conditions on Electron Trap Concentrations in Si-Doped $Al_{0.2}Ga_{0.8}As$ Grown by MBE", Jpn. J. Appl. Phys., Vol.23, L112, 1984.

22. P.K.Bhattacharya, T.Matsumoto, and S.Subramanian, "The Relation of Dominant Deep Levels in MOCVD $Al_xGa_{1-x}As$ with Growth Conditions", J. Crystal Growth, Vol.68, pp.301, 1984.

23. E.E.Wagner, D.E.Mar, G.Hom, and G.B.Stringfellow, "Deep Electron Traps in Organometallic Vapor Phase Grown $Al_xGa_{1-x}As$", J. Appl. Phys., Vol.51, pp.5434, 1980.

24. T.Matsumoto, P.K.Bhattacharya, and M.J.Ludowise, "Behavior of the 0.82 eV and Other Dominant Electron Traps in Organometallic Vapor Phase Epitaxy $Al_xGa_{1-x}As$", Appl. Phys. Lett., Vol.41, pp.662, 1982.

25. H.Kunzel, K.Ploog, K.Wunstel, and B.L.Zhou, "Influence of Alloy Composition, Substrate Temperature, and Doping Concentration on Electrical Properties of Si-Doped n-$Al_xGa_{1-x}As$ Grown by Molecular Beam Epitaxy", J. Electron. Mater., Vol.13, pp.281, 1984.

26. R.Magno, R.Shelby, N.D.Wilsey, S.M.Bedair, and J.Comas, "Deep Levels in Be Implanted GaAlAs", Inst. Phys. Conf. Ser., Vol.59, pp.431, 1981.

27. P.M.Mooney, R.Fischer, and H.Morkoc, "Transient Capacitance Study of Electron Traps in AlGaAs Grown with As_2", J. Appl. Phys., Vol.57, pp.1928, 1985.

28. C.E.Barnes, T.E.Zipperian, and L.R.Dawon, "Neutron-Induced Trapping Levels in Aluminum Gallium Arsenide", J. Electron. Mater., Vol.14, pp.95, 1985.

29. S.Subramanian, U.Schuller, and J.R.Arthur, Characterization of DX Centers in Molecular Beam Epitaxy Grown Si-Doped $Al_xGa_{1-x}As$ Using Schottky Barriers and Modulation Doped Field Effect Transistors", J. Appl. Phys., Vol.58, pp.845, 1985.

30. J. Engemann, "A.C. Admittance Stydies of Schottky Diodes Using a Vector Analyzer System", Solid State Electron., Vol.24, pp.467, 1981.

31. C. T. Sah, W. W. Chan, H. S. Fu, and J. W. Walker, "Thermally Stimulated Capacitance (TSCAP) in p-n Junctions", Appl. Phys. Lett., Vol.20, pp.193, 1972.

32. D. V. Lang, "Deep -Level Transient Spectroscopy: A New Method to Characterize Traps in Semiconductors", J. Appl. Phys., Vol.45, pp.3023, 1974.

33. F. Hasegawa, N. Iwata, and Y. Nannichi, "Relation between Cr-Level and Main Electron Trap (EL2) in Boat-Grown Bulk GaAs", Jpn. J. Appl. Phys., Vol.21, pp.1479, 1982.

34. S. M. Sze, "Physics of Semiconductor Devices", Second Edition, Jhon Wiley & son Inc., 1983.

35. Y. Zou, in GaAs and Related Compounds (1981), "On the Probable Nature of Certain Electron Traps in GaAs", Inst. Phys. Conf. Ser., Vol.63, pp.185, 1982.

36. E. R. Weber, H. Ennen, U. Kaufmann, J. Schneider, and T. Wosinski, "Identification of As_{Ga} Antisites in Plastically Deformed GaAs", J. Appl. Phys., Vol.53, pp.6140, 1982.

37. S. S. Li, D. H. Lee, and C. G. Choi, "Grown-in Defects in Multi-Epilayer GaAs Grown by NOCVD under Different Growth Conditions", Appl. Phys. Lett., to be published in December, 1985.

38. M. Taniguchi, and T. Ikoma, "Variation of the Midgap Electron Traps (EL2) in Liquid Encapsulated Czochralski GaAs", J. Appl. Phys., Vol.54, pp.6448, 1983.

39. D. S. Day, J. D. Oberstar, T. J. Drummond, H. Morkoc, A. Y. Cho, and B. G. Streetman, "Electron Traps Created by High Temperature Annealing in MBE n-GaAs", J. Electron. Mater., Vol.10, pp.445, 1981.

40. W. L. Wang, "Study of Grown-in Defects and Radiation-Induced Defects in GaAs and $Al_xGa_{1-x}As$", Ph.D. Dissertation, Dept. of Electrical Engineering, University of Florida, 1984.

41. P. A. martin, B. G. Streetman, and K. Hess, "Electric Field Enhanced Emission From Non-Coulombic Traps in Semiconductors", J. Appl. Phys., Vol.52, pp.7409, 1981.

42. A. Majerfeld, and K. Bhattacharya. "New Technique for Identification of Deep -Level Trap Emission to Indirect Conduction minima in GaAs", Appl.Phys. Lett., Vol.33, pp.259, 1978.

43. S. Adachi, "GaAs, AlAs, and $Al_xGa_{1-x}As$:Material Parameters for Used in Research and Device Applications", J. Appl. Phys., Vol.58, R1, 1985.

44. N.Lifshitz, A.Jayaraman, and R.A.Logan, "Pressure and Compositional Dependences of the Hall Coefficient in $Al_xGa_{1-x}As$ and Their Significance", Phys. Rev. B, Vol.21, pp.670, 1980.

45. P. D. Dapkus, "A Critical Comparison of MOCVD and MBE for Heterojunction Devices", J. Cryst. Growth, Vol.68, pp.345, 1984.

46. C. I. Huang, and S. S. Li, "Analysis of Transient Capacitance Experiments for Au-GaAs Schottky Barrier Diodes in the Presence of Deep Impurities and the Interfacial Layer", Solid State Electron., Vol.16, pp.1481, 1972.

47. G.M. Martin, A. Mitoneau, D. Pons, A. Mircea, and D. W. Woodard, "Detailed Electrical Characterization of the Deep Cr Acceptor in GaAs", J. Phys. C : Solid. St. Phys., Vol.13, pp.3855, 1980.

48. B. Tuck, G. A. Adegboyega, P. R. Jay, and M. J. Cardwell, "Out-diffusion of Chromium from GaAs Substrates", Inst. Phys. Conf. Ser., Vol.45, pp.114, 1979.

49. G. M. Martin, J. P. Farges, G. Jacob, and J. P. Hallais, "Compensation Mechanisms in GaAs", J. Appl. Phys., Vol.51, pp.2844, 1980.

50. H. Okamoto, and S. Sakata, "Depth Profile of Concentration of Deep Level Impurities in Vapor Phase Epitaxial Gallium Arsenide Grown under Various Arsenic Vapor Pressures", J. Appl. Phys., Vol.44, pp.1316, 1973.

51. G. Vincent, A. Chantre, and D. Bois, "Electric Field Effect on the Thermal Emission of Traps in Semiconductor Junctions", J. Appl. Phys., Vol.50, pp.5484, 1979.

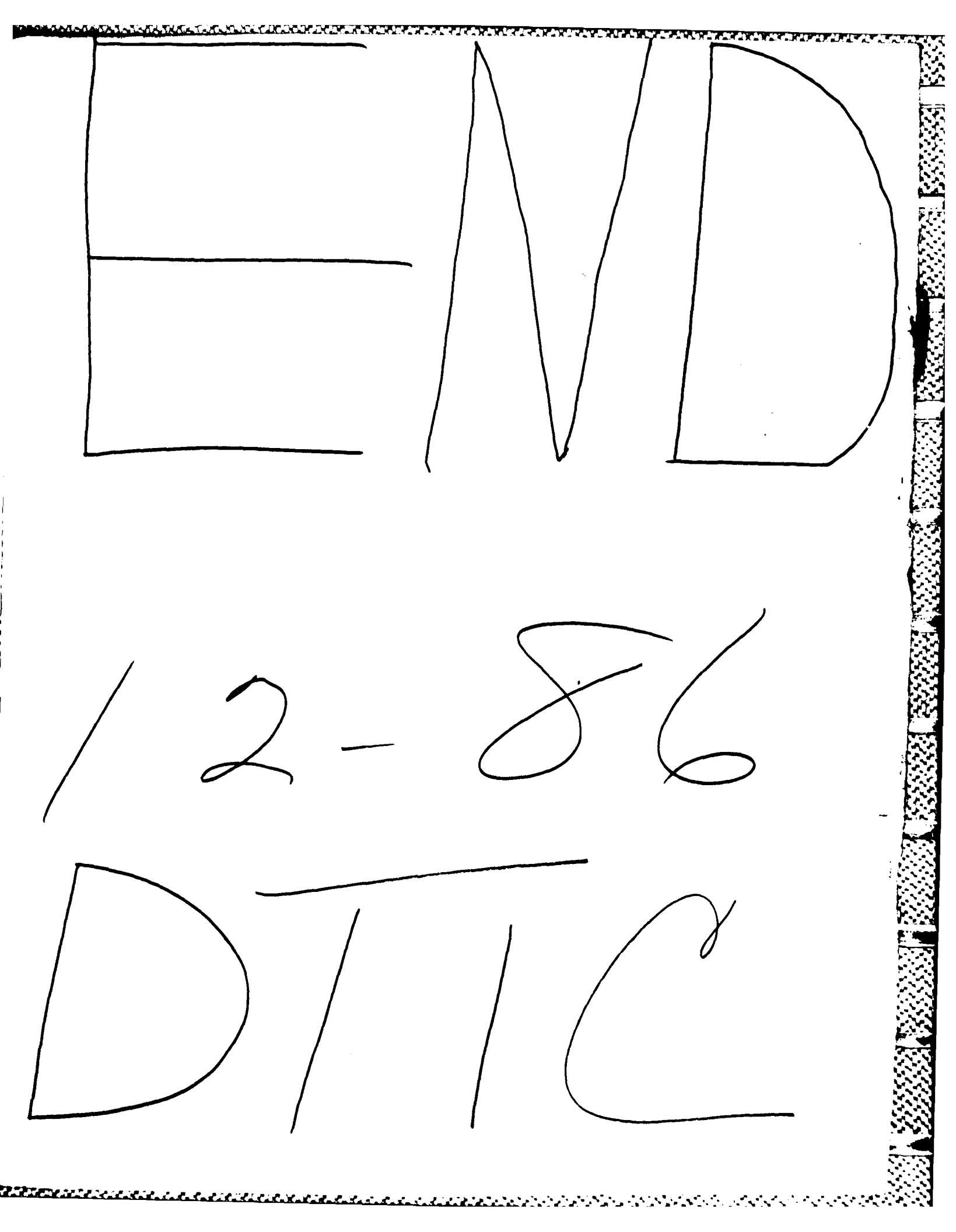
END
12-86
DTIC